J|A|C|S
ARTICLES
Published on Web 02/19/2002

Genesis of Nanostructured, Magnetically Tunable Ceramics from the Pyrolysis of Cross-Linked Polyferrocenylsilane Networks and Formation of Shaped Macroscopic Objects and Micron Scale Patterns by Micromolding Inside Silicon Wafers

Madlen Ginzburg,[†] Mark J. MacLachlan,[†,⊥] San Ming Yang,[†] Neil Coombs,[†] Thomas W. Coyle,[‡] Nandyala P. Raju,[§] John E. Greedan,[§] Rolfe H. Herber,[∥] Geoffrey A. Ozin,*[,†] and Ian Manners*[,†]

Contribution from the Polymer and Materials Chemistry Research Group, Department of Chemistry, University of Toronto, 80 St. George Street, Toronto, Ontario M5S 3H6, Canada, Department of Metallurgy and Materials Science and the Department of Chemical Engineering and Applied Chemistry, University of Toronto, 184 College Street, Toronto, Ontario M5S 3E4, Canada, Institute for Materials Research, McMaster University, Hamilton, Ontario L8S 4M1, Canada, and Racah Institute of Physics, The Hebrew University of Jerusalem, 91904 Jerusalem, Israel

Received March 19, 2001

Abstract: The ability to form molded or patterned metal-containing ceramics with tunable properties is desirable for many applications. In this paper we describe the evolution of a ceramic from a metal-containing polymer in which the variation of pyrolysis conditions facilitates control of ceramic structure and composition, influencing magnetic and mechanical properties. We have found that pyrolysis under nitrogen of a well-characterized cross-linked polyferrocenylsilane network derived from the ring-opening polymerization (ROP) of a spirocyclic [1]ferrocenophane precursor gives shaped macroscopic magnetic ceramics consisting of α-Fe nanoparticles embedded in a SiC/C/Si_3N_4 matrix in greater than 90% yield up to 1000 °C. Variation of the pyrolysis temperature and time permitted control over the nucleation and growth of α-Fe particles, which ranged in size from around 15 to 700 Å, and the crystallization of the surrounding matrix. The ceramics contained smaller α-Fe particles when prepared at temperatures lower than 900 °C and displayed superparamagnetic behavior, whereas the materials prepared at 1000 °C contained larger α-Fe particles and were ferromagnetic. This flexibility may be useful for particular materials applications. In addition, the composition of the ceramic was altered by changing the pyrolysis atmosphere to argon, which yielded ceramics that contain Fe_3Si_5. The ceramics have been characterized by a combination of physical techniques, including powder X-ray diffraction, TEM, reflectance UV−vis/near-IR spectroscopy, elemental analysis, XPS, SQUID magnetometry, Mössbauer spectroscopy, nanoindentation, and SEM. Micromolding of the spirocyclic [1]ferrocenophane precursor within soft lithographically patterned channels housed inside silicon wafers followed by thermal ROP and pyrolysis enabled the formation of predetermined micron scale designs of the magnetic ceramic.

Introduction

Ceramics, such as SiC and Si_3N_4, are important structural materials due to their strength and high-temperature resistance.[1−5] These ceramics are used in diverse applications such as automobile engines[1] and armor.[5] Traditional methods to prepare ceramics often require grinding the correct stoichiometry of elements and subsequent heating at extremely high temperatures greater than ca. 1500 °C.[1−3] The utility of these synthetic techniques is strongly dependent on the purity, composition, and particle size of the starting material.[4] Moreover, the resulting ceramics are obtained with little control over their morphology; the materials are usually isolated as powders and are heterogeneous at the microscopic level.[4]

Over the past decade there has been a transition in ceramic science from the traditional trial-and-error methods and extreme reaction conditions to softer, precursor-based methods.[4,6−14] The

[†] Polymer and Materials Chemistry Research Group, University of Toronto.
[‡] Department of Metallurgy and Materials Science, University of Toronto.
[§] McMaster University.
[∥] The Hebrew University of Jerusalem.
[⊥] Current address: Department of Chemistry, University of British Columbia, 2036 Main Mall, Vancouver, British Columbia V6T 1Z1, Canada.

(1) Narula, C. K. *Ceramic Precursor Technology and Its Applications*; Marcel Dekker: New York, 1995.
(2) Segal, D. *Chemical Synthesis of Advanced Ceramic Materials*; Cambridge University Press: New York, 1991.
(3) Phillips, G. C. *A Concise Introduction to Ceramics*; Van Nostrand Reinhold: New York, 1991.
(4) Baldus, H.-P.; Jansen, M. *Angew. Chem., Int. Ed. Engl.* **1997**, *36*, 328.
(5) Schwartz, M. *Handbook of Structural Ceramics*; McGraw-Hill: New York, 1992; p 8.31.
(6) Birot, M.; Pillot, J.-P.; Dunoguès, J. *Chem. Rev.* **1995**, *95*, 1443.
(7) For a review on preceramic routes to SiC, see: Laine, R. M.; Babonneau, F. *Chem. Mater.* **1993**, *5*, 260.
(8) Bill, J.; Aldinger, F. *Adv. Mater.* **1995**, *7*, 775.

use of polymer precursors in ceramic synthesis allows for control of the composition and properties of the resulting materials. Synthesis from a polymer network allows for atomic level mixing and, therefore, more homogeneous ceramics, better control over morphology, improved mechanical strength, enhanced physical properties, and retention of the shape of the processible polymer precursor providing the ceramic yield is high.[8] For example, in 1974, Winter and co-workers made SiC/Si_3N_4 fibers from polysilazane precursors.[9] Shortly thereafter, Yajima and co-workers obtained SiC (NICALON) fibers in 60% ceramic yield using polycarbosilane precursors.[10] More recently, Interrante and co-workers have made silicon carbide in 85% ceramic yield through the pyrolysis of a poly(silylenemethylene).[11] In addition, SiBNC ceramics have been prepared from the pyrolysis of boron-modified polysilazanes, and shaped ceramics were obtained from processible borane-functionalized hydridopolysilazanes.[12,13]

Most studies of ceramics formed from polymer precursors have focused on the mechanical and thermal properties of the material.[1−3] The incorporation of transition metals into such ceramics is desirable as it may introduce interesting magnetic, electrical, and optical properties.[14−23] Unfortunately, progress in this virtually unexplored area has been hindered by the synthetic difficulties associated with the preparation of well-defined polymers containing transition metals in the backbone which afford high ceramic yields.[15]

As ferrocene is a relatively cheap and tunable compound, the incorporation of ferrocenyl moieties into a polymer precursor is an attractive route toward the introduction of iron into a ceramic. Indeed, in the 1970s Yajima and Omori briefly reported the pyrolysis of a resin containing poly(acetylferrocene) to give a glassy matrix containing Fe particles.[16] In the past decade, ring-opening polymerization (ROP) of [1]silaferrocenophanes **1** has emerged as a convenient route to high-molecular weight polyferrocenylsilanes **2** (Scheme 1).[24,25] These well-characterized

Scheme 1

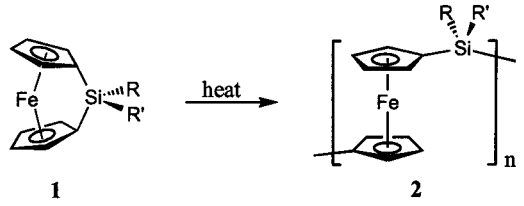

1 **2**

Scheme 2

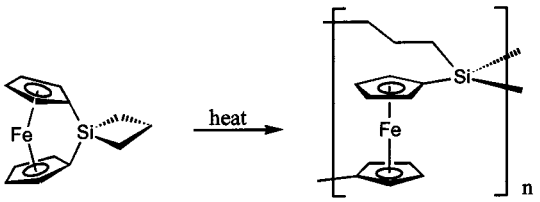

3 **4**

metal-containing polymers possess a variety of interesting properties that are dependent on the substituents R at the Si atom.[25] Earlier work showed that upon pyrolysis of these linear polymers (e.g., R = R′ = Me and R= R′ = Ph) at 1000 °C, ceramic materials containing ferromagnetic α-Fe crystallites embedded in a C/SiC/Si_3N_4 matrix were formed.[17,18] However, the ceramic yields (17−56%) were too low for shape retention.[18] More recently, Tang and co-workers have prepared ceramics in 48−62% yields containing α-Fe_2O_3 nanocrystals from a hyperbranched polyferrocenylsilane precursor.[19] In addition, pyrolysis of polyferrocenylsilanes inside mesoporous silica hosts has also recently been studied as a route to nanostructured magnetic materials.[20,21]

To enhance ceramic yields we have studied the pyrolysis of networks derived from spirocyclic [1]ferrocenophanes, which function as cross-linking agents. Spirocyclic compound **3** is readily obtained from the reaction of dilithioferrocene with dichlorosilacyclobutane.[26] We have previously demonstrated that **3** will copolymerize with **1** (R = R′ = Me) to form cross-linked polyferrocenylsilanes which form swellable gels and display improved ceramic yields.[27] When **3** was heated in a cylindrical Pyrex tube, a highly cross-linked network **4** formed (Scheme 2) that resembled the shape of the polymerization vessel.[28] In a preliminary report, we noted that network **4** can be pyrolyzed under a nitrogen atmosphere to afford Fe/SiC/C/Si_3N_4 ceramics **5** with shape retention in greater than 90% ceramic yield.[28] Through a combination of magnetic measurements, Mössbauer spectroscopy, and electron microscopy, we showed that the ceramics contain magnetic α-Fe nanoparticles.[28]

In this paper, we report detailed studies of the pyrolysis of polymer network **4**, including in-depth characterization of the α-Fe nanoparticles and the ceramic matrix. The growth of the α-Fe particles in a rigid polymer matrix creates a unique opportunity to control the particle size and to create a homogeneous distribution of particles. On the basis of analyses of

(9) Winter, G.; Verbeek, W.; Mansmann, M. German Patent 2,243,527, 1974; *Chem. Abstr.* **1974**, *81*, 126134.
(10) Yajima, S.; Hayashi, J.; Omori, M. *Chem. Lett.* **1975**, 931.
(11) Liu, Q.; Wu, H.-J.; Lewis, R.; Maciel, G. E.; Interrante, L. V. *Chem. Mater.* **1999**, *11*, 2038.
(12) (a) Wideman, T.; Cortez, E.; Remsen, E. E.; Zank, G. A.; Carroll, P. J.; Sneddon, L. G. *Chem. Mater.* **1997**, *9*, 2218. (b) Wideman, T.; Remsen, E. E.; Cortez, E.; Chlanda, V. L.; Sneddon, L. G. *Chem. Mater.* **1998**, *10*, 412.
(13) Weinmann, M.; Schuhmacher, J.; Kummer, H.; Prinz, S.; Peng, J.; Seifert, H. J.; Christ, M.; Müller, K.; Bill, J.; Aldinger, F. *Chem. Mater.* **2000**, *12*, 623.
(14) For a recent review on molecular and polymeric precursors to ceramics: Corriu, R. J. P. *Angew. Chem., Int. Ed.* **2000**, *39*, 1376.
(15) Manners, I. *Angew. Chem., Int. Ed. Engl.* **1996**, *35*, 1602.
(16) Yajima, S.; Omori, M. *Nature* **1977**, *267*, 823.
(17) Tang, B.-Z.; Petersen, R.; Foucher, D. A.; Lough, A. J.; Coombs, N.; Sodhi, R.; Manners, I. *J. Chem. Soc., Chem. Commun.* **1993**, 523.
(18) Petersen, R.; Foucher, D. A.; Tang, B.-Z.; Lough, A. J.; Raju, N. P.; Greedan, J. E.; Manners, I. *Chem. Mater.* **1995**, *7*, 2045.
(19) Sun, Q.; Lam, J. W. Y.; Xu, K.; Xu, H.; Cha, J. A. K.; Wong, P. C. L.; Wen, G.; Zhang, X.; Jing, X.; Wang, F.; Tang, B. Z. *Chem. Mater.* **2000**, *12*, 2617.
(20) (a) MacLachlan, M. J.; Aroca, P.; Coombs, N.; Manners, I.; Ozin, G. A. *Adv. Mater.* **1998**, *10*, 144. (b) MacLachlan, M. J.; Ginzburg, M.; Coombs, N.; Raju, N. P.; Greedan, J. E.; Ozin, G. A.; Manners, I. *J. Am. Chem. Soc.* **2000**, *122*, 3878.
(21) Another approach to the incorporation of metals into ceramics involves heating a preceramic organosilicon polymer with metal powders, oxides, or complexes. See for example: (a) Seyferth, D.; Czubarow, P. *Chem. Mater.* **1994**, *6*, 10. (b) Corriu, R. J. P.; Gerbier, P.; Guérin, C.; Henner, B. *Angew. Chem., Int. Ed. Engl.* **1992**, *31*, 1195.
(22) (a) Houser, E. J.; Keller, T. M. *Macromolecules* **1998**, *31*, 4038. (b) Corriu, R. J. P.; Devylder, N.; Guérin, C.; Henner, B.; Jean, A. *J. Organomet. Chem.* **1996**, *509*, 249. (c) Bourg, S.; Boury, B.; Corriu, R. J. P. *J. Mater. Chem.* **1998**, *8*, 1001.
(23) For a report on ceramics from iron carbonyl-containing polymers, see: Ungurenasu, C. *Macromolecules* **1996**, *29*, 7297.
(24) Foucher, D. A.; Tang, B.-Z.; Manners, I. *J. Am. Chem. Soc.* **1992**, *114*, 6246.
(25) (a) Manners, I. *Chem. Commun.* **1999**, 857. (b) Manners, I. *Can. J. Chem.* **1998**, *76*, 371. (c) Manners, I. *Pure Appl. Chem.* **1999**, *71*, 1471.
(26) MacLachlan, M. J.; Lough, A. J.; Geiger, W. E.; Manners, I. *Organometallics* **1998**, *17*, 1873.
(27) (a) Kulbaba, K.; MacLachlan, M. J.; Evans, C. E. B.; Manners, I. *Macromol. Chem. Phys.* **2001**, *202*, 1768. (b) MacLachlan, M. J.; Lough, A. J.; Manners, I. *Macromolecules* **1996**, *29*, 8562.
(28) MacLachlan, M. J.; Ginzburg, M.; Coombs, N.; Coyle, T. W.; Raju, N. P.; Greedan, J. E.; Ozin, G. A.; Manners, I. *Science* **2000**, *287*, 1460.

Table 1. Summary of Pyrolysis Conditions, Ceramic Yields, and Compositions

sample[a]	pyrolysis temp (°C)	pyrolysis time (h)	pyrolysis atmosphere	ceramic yield (%)[b]	ceramic composition by PXRD
$\mathbf{5D}_{500\,°C-2\,h}$	500	2	N_2	91.7	
$\mathbf{5D}_{550\,°C-2\,h}$	550	2	N_2	91.1	
$\mathbf{5D}_{600\,°C-2\,h}$	600	2	N_2	89.3[c]	α-Fe[c]
$\mathbf{5D}_{600\,°C-24\,h}$	600	24	N_2	90.1	α-Fe
$\mathbf{5D}_{650\,°C-2\,h}$	650	2	N_2	89.7	α-Fe
$\mathbf{5D}_{700\,°C-0\,h}$	700	0	N_2	89.0	α-Fe
$\mathbf{5D}_{700\,°C-2\,h}$	700	2	N_2	90.6	α-Fe, C (gr)
$\mathbf{5D}_{700\,°C-8\,h}$	700	8	N_2	91.5	α-Fe, C (gr)
$\mathbf{5D}_{700\,°C-12\,h}$	700	12	N_2	91.3	α-Fe, C (gr)
$\mathbf{5D}_{700\,°C-24\,h}$	700	24	N_2	92.1	α-Fe, C (gr)
$\mathbf{5D}_{750\,°C-2\,h}$	750	2	N_2	90.8	α-Fe, C (gr)
$\mathbf{5D}_{800\,°C-2\,h}$	800	2	N_2	90.9	α-Fe, C (gr)
$\mathbf{5D}_{850\,°C-2\,h}$	850	2	N_2	91.1	α-Fe, C (gr), Fe_4N
$\mathbf{5D}_{900\,°C-2\,h}$	900	2	N_2	93.0	α-Fe, C (gr), Fe_4N
$\mathbf{5D}_{950\,°C-2\,h}$	950	2	N_2	91.9	α-Fe, C (gr), α-Si_3N_4, Fe_4N, Fe_2N
$\mathbf{5D}_{1000\,°C-2\,h}$	1000	2	N_2	93.0[d]	α-Fe, C (gr), α-Si_3N_4, Fe_4N, Fe_2N[d]
$\mathbf{5D}_{1000\,°C-8\,h}$	1000	8	N_2	91.6	α-Fe, C (gr), α-Si_3N_4, Fe_4N, Fe_2N
$\mathbf{5D}_{1000\,°C-24\,h}$	1000	24	N_2	91.0	α-Fe, C (gr), α-Si_3N_4, Fe_4N, Fe_2N
$\mathbf{5F}_{550\,°C-1\,h}$	550	1	N_2		
$\mathbf{5P}_{600\,°C-2\,h}$	600	2	N_2	83.7	α-Fe
$\mathbf{5P}_{800\,°C-2\,h}$	800	2	N_2	88.9	α-Fe, C (gr)
$\mathbf{5P}_{1000\,°C-2\,h}$	1000	2	N_2	89.3	α-Fe, C (gr), α-Si_3N_4, Fe_4N, Fe_2N
$\mathbf{6}_{600\,°C-2\,h}$	600	2	Ar	81.3	α-Fe
$\mathbf{6}_{800\,°C-2\,h}$	800	2	Ar	88.6	Fe_5Si_3
$\mathbf{6}_{1000\,°C-2\,h}$	1000	2	Ar	86.7	Fe_5Si_3
$\mathbf{7}_{1000\,°C-2\,h}$	1000	2	Air	52.8	Fe_2O_3, SiO_2 (quartz)

[a] D = Disk; F = Film; P = Powder. [b] Typical polymer samples were ca. 0.2−1.0 g. [c] Elemental analysis (%): Si (11 ± 1), Fe (21 ± 2), C (54.4 ± 0.2), H (2.8 ± 0.2), N (0.6 ± 0.2). [d] Elemental analysis (%): Si (12 ± 1), Fe (23 ± 2), C (57.4 ± 0.2), N (6.1 ± 0.2).

samples prepared under controlled conditions and in-situ experiments, we propose a model for the evolution of the ceramic from the polymer matrix. We also describe for the first time the micron scale patterning of the magnetic ceramic. This was achieved by micromolding of the spirocyclic [1]ferrocenophane precursor **3**, subsequent ROP to the cross-linked polyferrocenylsilane network **4**, and pyrolysis to the magnetic ceramic **5**, all conducted within soft lithographically patterned and anisotropically etched microchannels inside silicon wafers.

Experimental Section

Synthesis of Monomer 3 and Polymer Network 4. Spirocyclic [1]ferrocenophane **3** was synthesized according to the literature procedure.[26] The monomer was recrystallized from hexanes and then sublimed until it was pure by ^{1}H NMR spectroscopy. Monomer **3** was loaded into a Pyrex polymerization tube and sealed under vacuum. The sample was treated at 150 °C for 24 h and then at 180 °C for 24 h. After cooling to 25 °C, the tube was opened to yield the resulting cross-linked polymer **4**, which had taken the shape of the polymerization tube and appeared as a red rod-shaped solid. Using a blade, the polymer rod was cut into ca. 8 mm thick disks of ca. 10 mm diameter. Polymer films were formed by sublimation of the monomer onto a hot glass tube and were then peeled off to give free-standing films.

Data for 4. ^{1}H MAS NMR: 3.9 (Cp), 1.8 (CH_2) ppm. ^{13}C CP-MAS NMR: 18 (CH_2), 26 (CH_2), 63.8 (*ipso*-Cp), 66.5 (*ipso*-Cp), 67.6 (*ipso*-Cp), 73.2−76 (Cp) ppm. ^{29}Si CP-MAS NMR: 4 (s, $fcSi(CH_2)_3$), 9 ppm (br, $fc_xSi(CH_2)_{4-x}$ x = 2 or 3). UV−vis/NIR: 302 and 458 nm (d−d absorptions), 1666 and 1773 nm (C−H stretch first overtone).

Synthesis of Magnetic Ceramics 5, 6, and 7. The ceramics were all prepared from **4** by the same method. The synthesis of ceramic $\mathbf{5D}_{500\,°C-2\,h}$ is given as a representative preparation. A disk-shaped sample of polymer **4** (0.819 g) was placed in a quartz boat inside a quartz tube in a pyrolysis oven. The oven used was a 3-zone Lindberg pyrolysis oven described in ref 18. The tube was purged with nitrogen (99.999% prepurified from Matheson), and then the flow was adjusted to ca. 50 mL min^{-1}. The temperature in the pyrolysis oven was raised to 500 °C in 1 h and held constant for 2 h. After the tube furnace had cooled to room temperature under a flow of N_2 (cooling typically occurred over a period of ca. 6 h), the brown ceramic was removed and weighed. The ceramic (0.751 g, 91.7%) retained the disk shape of the starting polymer. The pyrolysis conditions and yields of the ceramics are summarized in Table 1. Ceramics **5D** (**D**isk) were all prepared in a similar fashion and differed only in the pyrolysis temperatures and heating times, where pyrolysis was performed on ca. 0.2−1.0 g polymer samples. Ceramic **5F** (**F**ilm) was prepared by performing pyrolysis on a free-standing polymer film. Ceramics **5P** (**P**owder) were prepared by pyrolysis of powdered polymer samples that were ground using a mortar and pestle. The average particle size of the powder was ca. 140 μm as measured from SEM images of the ground precursor. Ceramics **6** and **7** were prepared by pyrolysis of disk-shaped polymers under argon and air, respectively, as noted in Table 1.

Microcontact Printing. Fabrication of patterned Si(100) wafers by microcontact printing self-assembled monolayers (SAMs) of alkanethiols on gold followed by selective wet etching was adapted from literature procedures.[29] The line pattern poly(dimethylsiloxane) (PDMS) master was formed by curing the prepolymer gel (Sylgard 184, Corning) over a lithographic photoresist pattern at 60 °C for 8 h. The PDMS master was inked with a hexadecanethiol-ethanol solution (0.2 mM), dried under a flow of N_2 for 30 s, and then put into conformal contact with a Au (50 nm)-coated Si(100) wafer (5 nm Ti adhesion layer) for 5−10 s. The bare Au was then removed through selective etching (1 M KOH, 0.1 M $Na_2S_2O_3$, 0.01 M $K_3Fe(CN)_6$, 0.001 M $K_4Fe(CN)_6$), and the underlying Ti layer was removed using a 1% HF solution. Anisotropic etching of Si(100) was achieved using a 4 M KOH in H_2O/^{i}PrOH (3:1 v/v) solution at 70 °C for 10 min. After Si etching, the remaining metals were removed using aqua regia.

The Si substrates were cleaned with CCl_4, ^{i}PrOH, and finally with H_2O. The substrates were then sonicated in a piranha solution (H_2SO_4/H_2O_2; 4:1 v/v) for 1 h and washed with copious amounts of water. To

(29) (a) Xia, Y.; Rogers, J. A.; Paul, K. E.; Whitesides, G. M. *Chem. Rev.* **1999**, *99*, 1823. (b) Xia, Y.; Whitesides, G. M. *Adv. Mater.* **1996**, *8*, 765. (c) Xia, Y.; Zhao, X.-M.; Whitesides, G. M. *Microelectron. Eng.* **1996**, *32*, 255. (d) Xia, Y.; Zhao, X.-M.; Kim, E.; Whitesides, G. M. *Chem. Mater.* **1995**, *7*, 2332. (e) Kumar, A.; Biebuyck, H. A.; Whitesides, G. M. *Langmuir* **1994**, *10*, 1498.

remove adsorbed water, the substrates were heated to 200 °C under vacuum for 12 h. A film of monomer **3** on the Si substrate was prepared in the glovebox by dropping a concentrated solution of **3** in CH_2Cl_2 on the patterned substrate and allowing the solvent to evaporate. ROP of the film of monomer **3** to obtain polymer **4** was accomplished by heating the monomer-coated substrate to 200 °C for 12 h under N_2. The substrate was then placed in a 1 wt % HF solution for 5 days to etch away the silicon dioxide layer between the silicon substrate and polymer film, after which time the polymer film floated off the substrate. A piece of the patterned polymer film was pyrolyzed at 600 °C for 2 h in a manner similar to that described above. This created a magnetic ceramic replica of the patterned polymer precursor film.

Solid-State NMR Spectroscopy. The 400.10 MHz ^{1}H MAS, 100.63 MHz ^{13}C CP-MAS, and 79.49 MHz ^{29}Si CP-MAS NMR spectra were obtained on a Bruker DSX400 spectrometer. All samples were spun at 5 kHz. The ^{1}H NMR spectra were collected with a 1 s recycle delay time, while the ^{13}C and ^{29}Si NMR spectra were collected with a 10 s recycle delay and 5 ms contact time. ^{1}H, ^{29}Si, and ^{13}C NMR spectra were referenced to TMS ($Si(CH_3)_4$), $Si(Si(CH_3)_3)_4$ (−9.885 ppm vs TMS), and glycine (175.8 ppm vs TMS), respectively.

Powder X-ray Diffraction (PXRD) Studies. PXRD patterns were obtained on a Siemens D5000 X-ray diffractometer using Ni-filtered Cu Kα radiation ($\lambda = 1.54178$ Å).

TEM and SEM. Transmission electron micrographs were obtained with a Phillips 430 microscope operating at 100 kV. The samples were microtomed using a diamond knife into thin (ca. 300 Å) sections. Field emission TEM was performed on a JEOL 210F field emission microscope operating at an accelerating voltage of 200 kV. SEM images were obtained on a Hitachi S-570 microscope using an operating voltage of 15 kV.

Reflectance UV−Vis/Near-IR Spectroscopy. Spectra were obtained on a Perkin-Elmer Lambda 900 UV−vis/near-IR spectrometer equipped with a diffuse reflectance integrating sphere. Powdered samples were ground using a mortar and pestle and pressed into disks between quartz plates for data collection.

Elemental Analyses. Elemental analysis was performed by Galbraith Laboratories, Inc., Knoxville, TN on freshly ground samples.

XPS. Data were obtained using a Laybold MAX 200 XPS instrument. The X-ray source was a Mg anode operating at 15 kV and 20 μA or an Al anode operating at 15 kV and 25 μA. Freshly ground samples were mounted on double-sided copper tape. Data collection was performed under pressures of less than 1×10^{-6} Torr. Spectra were calibrated to the position of the carbon 1s peak at 284.6 eV.

Mössbauer Spectroscopy. The ceramic samples were crushed in an agate mortar and transferred to a plastic sample holder which was, in turn, introduced into the Mössbauer spectrometer. Spectra were obtained in transmission geometry, using a ca. 100 mCi source of ^{57}Co(Rh). Temperature control was effected using a large gain feed-back controller, and temperatures are considered accurate to better than ±0.2 K. All isomer shifts are reported with respect to the centroid of a room-temperature spectrum of α-Fe, which was also used to calibrate the spectrometer. Data reduction was effected using a least-squares matrix inversion routine with line positions, line widths, intensities, and background corrections as free parameters.

Magnetization Measurements. Magnetic measurements were carried out using a Quantum Design (MPMS), Superconducting Quantum Interference Device (SQUID) magnetometer, at 100 and 300 K.

Nanoindentation. Mechanical measurements were performed on a CSEM instrument using a Vickers diamond indenter. Samples were mounted in an epoxy resin and polished with SiC sandpaper (120−1200 coarse). Young's modulus and Vickers hardness were calculated using the Oliver-Pharr data analysis procedure.[30] The Poisson coefficient for the sample was estimated as 0.3, and the Young's modulus and the Poisson coefficient for the diamond indenter were 1141 GPa and 0.07, respectively.[31]

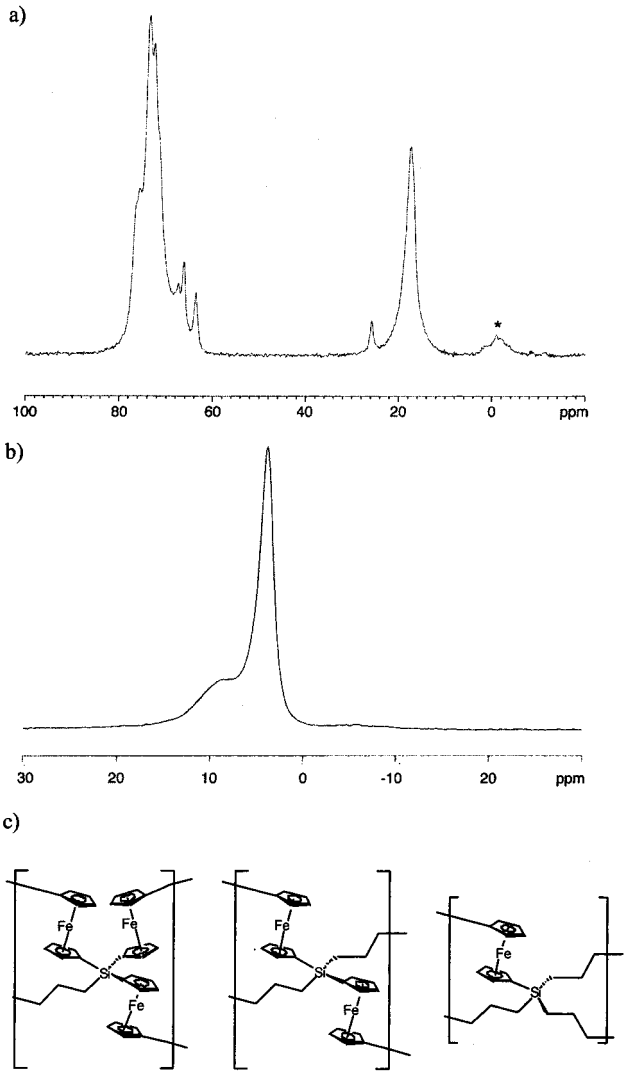

Figure 1. CP-MAS NMR (a) ^{13}C and (b) ^{29}Si spectra of polymer **4**. (c) The three possible Si microenvironments in the cross-linked polymer network **4**. (* represents a spinning side-band.)

Results and Discussion

1. Synthesis and Characterization of Cross-Linked Polyferrocenylsilane Network 4: Pyrolysis to Yield Shaped Macroscopic Magnetic Ceramics. The spirocyclic [1]ferrocenophane **3** was polymerized in a cylindrical Pyrex tube to yield polymer **4** as a red, rigid rod that retained the shape of the Pyrex former. ^{1}H magic angle spinning (MAS) NMR spectroscopy of polymer **4** showed two peaks centered at 3.9 and 1.8 ppm, attributed to the Cp and methylene resonances, respectively. Figure 1a shows the ^{13}C cross-polarization (CP)-MAS NMR spectrum of **4**; there are two resonances associated with the methylene groups of the carbosilane at 18 and 26 ppm. Downfield from these, several peaks were observed between 73 and 76 ppm, consistent with cyclopentadienyl (Cp) carbon atoms (C−H). Also, three resonances observed at 63.8, 66.5, and 67.6 ppm are assigned to *ipso*-Cp carbon atoms (C−Si), downfield from the single *ipso*-Cp resonance observed in the

(30) (a) Pharr, G. M. *Mater. Sci. Eng.* **1998**, *A253*, 151. (b) Oliver, W. C.; Pharr, G. M. *J. Mater. Res.* **1992**, *7*, 1564.
(31) Simmons, G.; Wang, H. *Single-Crystal Elastic Constants and Calculated Aggregate Properties: A Handbook*, 2nd ed.; MIT Press: Cambridge, MA, 1971.

Figure 2. (a) Photograph of a red polymer rod **4** (bottom) and the corresponding pyrolysis product, ceramic **5** (top). (b) Pentagon-shaped polymer **4** (bottom) and the resulting pentagon-shaped ceramic **5** (top).

strained monomer **3** at 31.9 ppm. The ^{29}Si CP-MAS NMR spectrum of **4** displayed a sharp peak at 4 ppm and a broader peak at 9 ppm, as shown in Figure 1b.

These NMR observations are consistent with the presence of three Si microenvironments. Assuming that the thermal ROP of **3** proceeds through random ring-opening of both the ferrocenophane and the silacyclobutane rings creating reactive Cp and CH_2 termini, and these can recombine with any other Si center, three Si microenvironments are expected, as illustrated in Figure 1c. This should lead to three distinct *ipso*-Cp resonances in the ^{13}C NMR spectrum of the **4** (Figure 1a). Furthermore, the sharp and broad peaks observed in the ^{29}Si CP-MAS NMR spectrum are also in accord with this model.

Pyrolysis of shaped polymer samples **4** in a tube furnace at 500−1000 °C under a flow of nitrogen afforded ceramics **5** in 91 ± 2% yield with shape retention. The high ceramic yield and shape retention are illustrated in Figure 2a with a photograph of a ceramic rod (top) formed from the pyrolysis of a polymer rod (bottom). Figure 2b shows a sample of polymer **4** (bottom) formed inside a pentagonal Teflon mold and the corresponding ceramic (top). It should be emphasized that the ceramics retained the shapes of the original polymers even though the pyrolyses were not performed in molds. Interestingly the macroscopic shaped ceramics were attracted to a bar magnet. We therefore performed an in-depth characterization of these materials and studied their formation in detail.

2. Genesis of Magnetic Ceramic 5: Systematic Studies as a Function of Pyrolysis Temperature and Time. To explore the evolution of the polymer to ceramic (**4** to **5**) transformation, we systematically varied pyrolysis temperatures and times under N_2 to study the growth of α-Fe nanoparticles within their surrounding matrix. The sample identification and pyrolysis conditions are summarized in Table 1. Ceramic samples **5D** (**D**isk), **5P** (**P**owder), and **5F** (**F**ilm) were prepared by pyrolysis of disk-shaped polymer samples, powdered polymer samples, and a free-standing polymer film, respectively. Pyrolysis temperatures were varied from 500 to 1000 °C, and pyrolysis times were varied from 0 h (heating the sample to the set temperature and then immediately allowing it to cool) to 24 h at selected temperatures.

2.a. Variation of Pyrolysis Temperature. To study the growth of the α-Fe particles in their surrounding matrix, ceramic samples were prepared at temperatures between 500 and 1000 °C. Each sample was heated to the respective temperature in 1 h, maintained for 2 h, then allowed to cool in the tube furnace under a flow of N_2. The final ceramics were light brown when prepared at 500 °C, with darker shades of brown observed with increasing temperatures until black materials were formed at 700 °C and higher. The bulk density of the ceramic prepared at 600 °C was determined to be 1.61 ± 0.01 g cm^{-3} by flotation, only slightly more dense than the polymer precursor **4** (1.54 g cm^{-3}). The resulting ceramic products were investigated by PXRD, TEM, reflectance UV−vis/near-IR, elemental analysis, X-ray photoelectron spectroscopy (XPS), superconducting quantum interference device (SQUID) magnetometry, Mössbauer spectroscopy, nanoindentation, and scanning electron microscopy (SEM).

2.a.i. Powder X-ray Diffraction Studies. PXRD patterns of polymer **4** and ceramics $\mathbf{5D_{(500-1000\,^{\circ}C)-2\,h}}$ prepared using variable temperatures (pyrolysis at 500−1000 °C for 2 h) are shown in Figure 3. The PXRD of the polymer network **4** showed two sharp peaks at $2\theta = 11°$, $d = 6.98$ Å and $2\theta = 13°$, $d = 5.84$ Å, corresponding to preferred Fe- - -Fe distances in the network. With increased pyrolysis temperatures, the structure of the polymer network and short-range order were lost as Fe atoms aggregated into α-Fe nanoparticles. The (110) reflection of α-Fe emerged as a broad halo ($2\theta = 45°$, $d = 2.03$ Å) at 600 °C ($\mathbf{5D_{600\,^{\circ}C-2\,h}}$). This peak sharpened at 700 °C ($\mathbf{5D_{700\,^{\circ}C-2\,h}}$) indicating the presence of crystalline α-Fe nanoparticles. The peak assigned to the (110) reflection of α-Fe became narrower and more intense as the pyrolysis temperature increased. The formation of large α-Fe particles was attributed to enhanced Fe mobility in the matrix above 700 °C. Presumably above this temperature Si−C and C−C bond cleavage readily occurs facilitating matrix rearrangement and Fe mobility.

Crystallization of the matrix surrounding the α-Fe nanoparticles was first observed at 700 °C with the appearance of the (002) reflection of graphite at $2\theta = 26°$, $d = 3.37$ Å in $\mathbf{5D_{700\,^{\circ}C-2\,h}}$. It should be noted that graphite crystallized at the same temperature that crystalline α-Fe appeared (700 °C). Progressive narrowing of the (002) reflection of graphite was observed with increasing temperature, and the crystallinity improved up to 1000 °C. The temperature at which graphite initially formed, 700 °C ($\mathbf{5D_{700\,^{\circ}C-2\,h}}$), was relatively low when compared to 1500−2100 °C required to form pyrolytic graphite

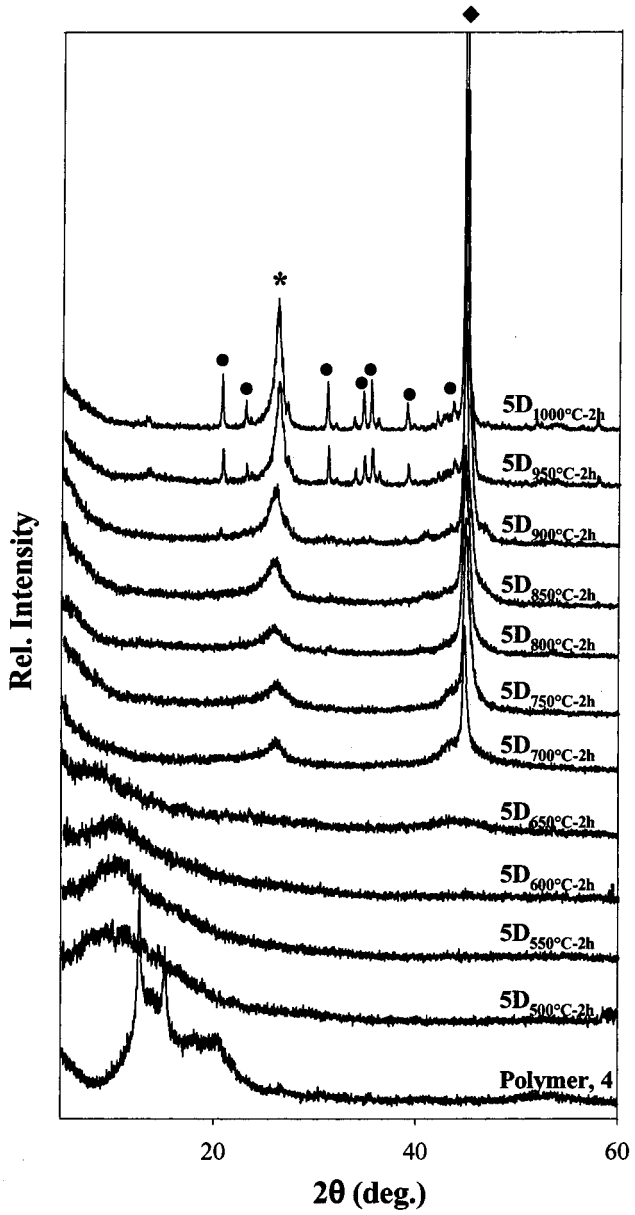

Figure 3. PXRD patterns of polymer **4** and ceramic samples $\mathbf{5D_{(500-1000\,^{\circ}C)-2\,h}}$ prepared at temperatures between 500 and 1000 °C. Temperatures increase from bottom to top. The crystalline species observed were α-Fe (◆), graphite (*), α-Si_3N_4 (●), Fe_4N, and Fe_2N.

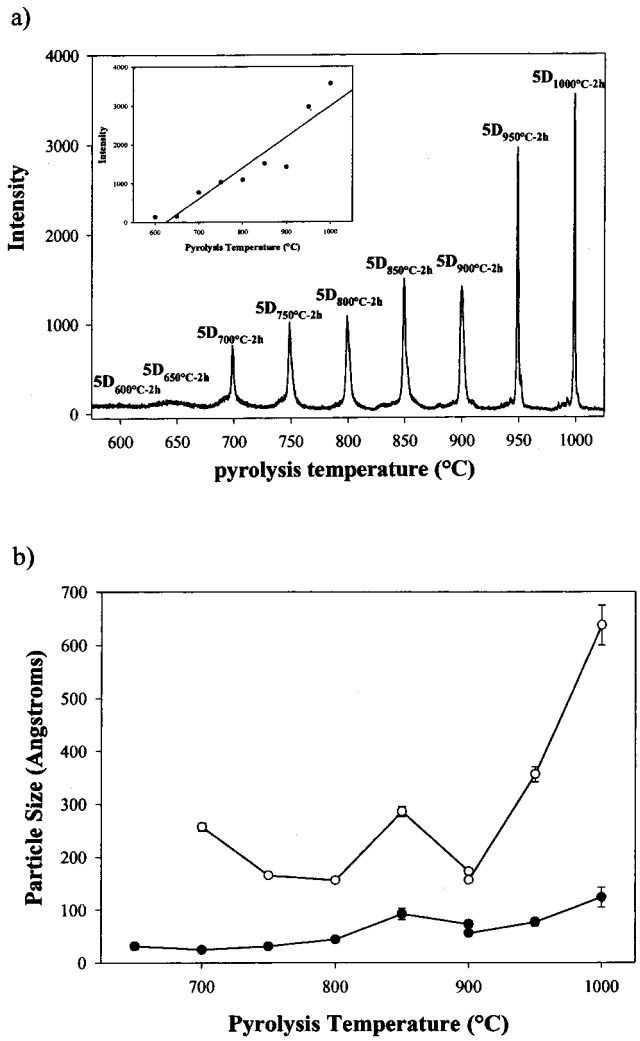

Figure 4. (a) PXRD patterns of the (110) α-Fe reflection from ceramics $\mathbf{5D_{(600-1000\,^{\circ}C)-2\,h}}$, prepared at 600 °C (left) to 1000 °C (right), with 50 °C temperature increments. The inset shows a plot of the pyrolysis temperature versus the intensity of the (110) α-Fe reflection for the same ceramic samples. (b) Graph of α-Fe particle size as a function of pyrolysis temperature for large crystalline particles (top) and small particles (bottom). The bimodal particle size distribution was observed for ceramics $\mathbf{5D_{(700-1000\,^{\circ}C)-2\,h}}$ prepared above 700 °C.

from thermal decomposition of hydrocarbons.[32] The low temperature formation and crystallization of graphite in this system may be catalyzed by α-Fe nanoparticles. Indeed, Rao et al. have previously observed the formation of carbon nanotubes catalyzed by Fe nanoparticles formed from the pyrolysis of ferrocene at 1100 °C.[33]

A small peak due to Fe_4N ((111) $d = 2.19$ Å) emerged in ceramics prepared at 850 °C ($\mathbf{5D_{850\,^{\circ}C-2\,h}}$) and higher. When the temperature reached 950 °C, α-Si_3N_4 and crystalline Fe_2N ((211) $d = 2.11$ Å) were observed as well as additional reflections for Fe_4N indicating an increased degree of crystallinity (α-Fe, graphite and α-Si_3N_4 were also observed when polymer **2** (R = R′ = Me) was pyrolyzed at 1000 °C).[18] It is interesting to note that the original precursor polymer **4** did not contain nitrogen. Therefore, the nitrogen present in the final ceramic was incorporated from the pyrolysis atmosphere. The silicon nitrides and iron nitrides also showed enhanced crystallinity with increased temperature as demonstrated by progressive growth of peak intensities.

Figure 4a shows the (110) reflection of α-Fe as a function of temperature. The observed increase in peak intensity demonstrates the growth of α-Fe particles. A plot of the intensity of the (110) α-Fe reflection versus pyrolysis temperature is shown in the inset of Figure 4a. There was an increase in the intensity with the exception of ceramic $\mathbf{5D_{900\,^{\circ}C-2\,h}}$, which was prepared at 900 °C. The deviation at 900 °C may be attributed to the observed formation of iron nitrides from reaction of surface α-Fe particles with the nitrogen atmosphere at this temperature (vide infra).

Analysis of the (110) reflection of α-Fe showed that at every pyrolysis temperature above 700 °C the reflection contained both a sharp high intensity and a broad low intensity component.

(32) Mantell, C. L. *Carbon and Graphite Handbook*; Interscience Publishers: New York, 1968; pp 162−170.
(33) Rao, C. N. R.; Sen, R.; Satishkumar, B. C.; Govindaraj, A. *Chem. Commun.* **1998**, 1525.

Table 2. Scherrer Analysis of the (110) α-Fe Reflection and the Corresponding α-Fe Particle Sizes for Ceramics Prepared at Various Pyrolysis Temperatures

ceramic sample[a]	pyrolysis temp[b](°C)	α-Fe particle size calculated from the (110) α-Fe reflection using the Scherrer equation (Å)[d]	
		small particles	large particles
5D$_{500\ °C-2\ h}$	500		
5D$_{550\ °C-2\ h}$	550		
5D$_{600\ °C-2\ h}$	600	*c*	
5D$_{650\ °C-2\ h}$	650	31 ± 6	
5D$_{700\ °C-2\ h}$	700	24.3 ± 0.7	257 ± 8
5D$_{750\ °C-2\ h}$	750	31 ± 1	165 ± 3
5D$_{800\ °C-2\ h}$	800	44 ± 2	156 ± 3
5D$_{850\ °C-2\ h}$	850	92 ± 11	286 ± 9
5D$_{900\ °C-2\ h}$	900	73 ± 7	173 ± 4
		56 ± 4	156 ± 3
5D$_{950\ °C-2\ h}$	950	77 ± 7	357 ± 14
5D$_{1000\ °C-2\ h}$	1000	123 ± 19	637 ± 37
5P$_{600\ °C-2\ h}$	600	78 ± 8	
5P$_{800\ °C-2\ h}$	800	160 ± 31	252 ± 8
5P$_{1000\ °C-2\ h}$	1000	205 ± 51	606 ± 34

[a] D = Disk; P = Powder. [b] Two hour pyrolysis time. [c] The (110) α-Fe reflection for **5D$_{600\ °C-2\ h}$** appeared as a weak, broad halo. Consequently, it was not possible to measure the fwhm to calculate an average particle size. [d] The errors obtained for the values of fwhm (from the peak fitting software, Peakfit) were used to estimate the errors for the particle size values.

This implied that each sample prepared above 700 °C contained a bimodal particle size distribution; small α-Fe nanoparticles contributed to the broader peak, while larger α-Fe crystallites contributed to the sharper peaks. For each of these samples, the sharp and broad (110) α-Fe reflections were resolved into their respective components, and the full width at half-maximum (fwhm) for each component was obtained.

As the Bragg reflections of nanoparticles smaller than ca. 1000 Å are broadened, the average size of α-Fe crystallites can be calculated from the fwhm values using the Scherrer equation.[34] The calculated α-Fe particle sizes of the small and large crystalline α-Fe nanoparticles are summarized in Table 2. The size of α-Fe nanoparticles versus pyrolysis temperature, for both the large and the small α-Fe particles, is plotted in Figure 4b. A linear increase in size was seen with an increase in temperature for the small α-Fe particles. This is contrasted with the larger α-Fe particles, which followed more rapid growth. One possible explanation for this trend is that the larger α-Fe particles formed at grain boundaries and defect sites within the ceramic matrix, where interparticle diffusion is fastest. The sample prepared at 900 °C was a reproducible exception to the trend as the size of both the large and the small α-Fe particles decreased. The observed decrease in particle size may be due to the formation of iron nitrides above 850 °C, which competes with the α-Fe nanoparticles for Fe atoms.

2.a.ii. TEM Studies. The temperature dependence of the α-Fe particle size was also monitored using TEM. Figure 5a−e shows TEM images of the ceramics prepared at every 100 °C between 600 and 1000 °C. For the sample prepared at 600 °C, no α-Fe particles were visible, and the matrix appeared homogeneous. By 700 °C, there were distinct small and large α-Fe particles present as well as graphitic ribbons. As the temperature was further increased, α-Fe particles visibly increased in size, maintaining a distribution of particle sizes. As expected from the PXRD observations, there was no observed significant increase in α-Fe particle size at 900 °C (**5D$_{900\ °C-2\ h}$**) as compared with that at 800 °C (**5D$_{800\ °C-2\ h}$**) due to the formation of Fe_4N, whereas α-Fe particle size visibly increased again at 1000 °C. These TEM observations are in good agreement with the PXRD results.

2.a.iii. Influence of Morphology on the Pyrolytic Evolution of 4. To study the importance of the morphology of the ceramic precursor **4** on the composition of the final ceramic, powdered samples **5P** were prepared by pyrolyzing powdered samples of polymer **4**. TEM images of ceramics **5P** showed small α-Fe particles at 600 °C (**5P$_{600\ °C-2\ h}$**) and bimodal particle size distributions at 800 °C (**5P$_{800\ °C-2\ h}$**) and 1000 °C (**5P$_{1000\ °C-2\ h}$**) as observed previously with ceramics **5D**. Average particle sizes calculated from the PXRD for these samples are given in Table 2. At 600 °C larger particles were present in the powdered sample **5P$_{600\ °C-2\ h}$** (78 ± 8 Å) as compared to those of **5D$_{600\ °C-2\ h}$** (which were too small to calculate an average particle size). This difference may be attributed to an increased surface area and population of grain boundaries, leading to faster Fe diffusion and controlled nanoparticle growth in the powder. Similarly, **5P$_{800\ °C-2\ h}$** prepared by pyrolysis of a powder has larger particles (160 ± 31 Å and 252 ± 8 Å) than does **5D$_{800\ °C-2\ h}$** prepared by bulk pyrolysis of a disk at 800 °C (44 ± 2 Å and 156 ± 3 Å). At 1000 °C the particle sizes for **5P$_{1000\ °C-2\ h}$** are similar to the particles in **5D$_{1000\ °C-2\ h}$**. The difference in surface area between the powder and disk becomes less significant at 1000 °C.

The formation of a ceramic film (**5F**) from a free-standing polymer film was also studied. Figure 5f shows the TEM image for ceramic sample **5F$_{550\ °C-1\ h}$**. At this temperature the formation of iron nanoparticles of low polydispersity is clearly evident. The formations of α-Fe particles in **5F** at a lower temperature than in the bulk may be associated with enhanced mobility of Fe atoms in the thin film.

2.a.iv. Studies by Reflectance UV−Vis/Near-IR Spectroscopy, Elemental Analysis, and XPS. UV−vis/near-IR spectroscopy proved useful in elucidating the fate of the ferrocene moieties in polymer network **4** during ceramic formation.[35] We observed two d−d absorptions for the ferrocenyl groups in the polymer **4** at 302 and 458 nm. These absorptions diminished in samples prepared at 500 °C (**5D$_{500\ °C-2\ h}$**) and completely disappeared by 650 °C (**5D$_{650\ °C-2\ h}$**). Additionally, the C−H stretching overtone present in the polymer at 1666 nm (6002 cm^{-1}) showed a similar trend. This suggests that the ferrocene moieties had completely decomposed by 600 °C. With increased pyrolysis temperatures, the UV−vis/near-IR spectral curves showed increased absorption throughout the spectral region, probably due to enhanced metallic character of the ceramics.

Elemental analysis was performed on representative ceramics **5D$_{600\ °C-2\ h}$** and **5D$_{1000\ °C-2\ h}$** (Table 1). The ceramic prepared at 600 °C had one-half as much hydrogen as the precursor **4**, and the ceramic prepared at 1000 °C did not contain any hydrogen. These results are consistent with the observed decrease in the C−H stretch in the UV−vis/near-IR at 600 °C and its disappearance above 650 °C. As expected, the amount of nitrogen incorporated into the ceramics increased significantly with temperature (0.6% in **5D$_{600\ °C-2\ h}$** and 6.1% in **5D$_{1000\ °C-2\ h}$**) indicating the presence of a significant amount of Si_3N_4 at 1000 °C.

(34) Cullity, D. B. *Elements of X-ray Diffraction*, 2nd ed.; Addison-Wesley Publishing Company Inc.: Reading, MA, 1978; p 284.

(35) See Supporting Information for further details.

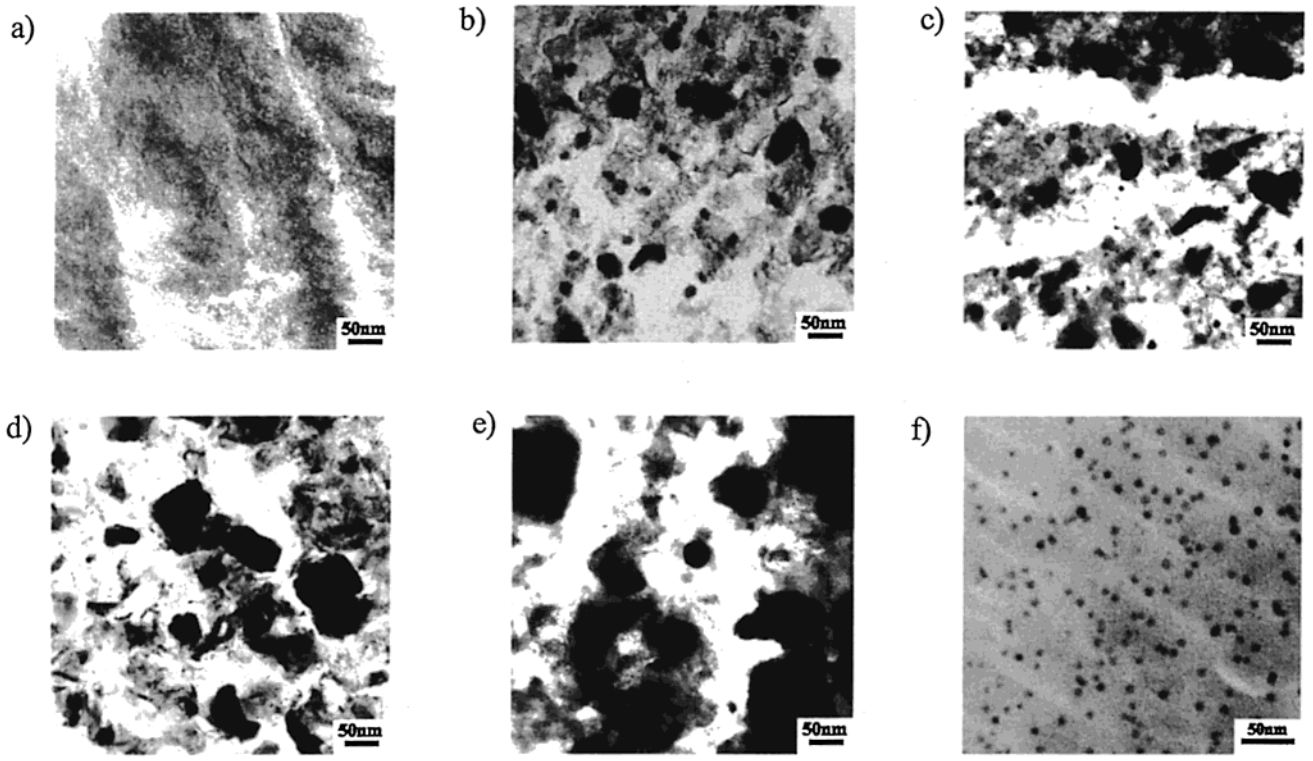

Figure 5. TEM images of ceramics prepared at (a) 600 °C (**5D**$_{600\ °C-2\ h}$); (b) 700 °C (**5D**$_{700\ °C-2\ h}$); (c) 800 °C (**5D**$_{800\ °C-2\ h}$); (d) 900 °C (**5D**$_{900\ °C-2\ h}$); and (e) 1000 °C (**5D**$_{1000\ °C-2\ h}$). (f) TEM micrograph of ceramic film **5F**$_{550\ °C-1\ h}$.

We investigated the ceramics using XPS to identify the surface composition.[35] Examination of the Fe2p$_{3/2}$ region indicated that the relative amount of Fe detected on the external surface of the material decreased as the pyrolysis temperature increased. The amount of Fe on the external surface of the material presumably decreases as Fe atoms are released from polymeric ferrocene moieties and migrate through the matrix to form α-Fe particles. In addition, nitrogen was detected on the ceramic surface with the appearance of the N1s peak at 700 °C (**5D**$_{700\ °C-2\ h}$), followed by a subsequent intensity increase with pyrolysis temperature. At 700 °C the N1s peak represented a binding energy (E_B) of 398 eV, which agrees well with that of amorphous Si_3N_4.[36] Similarly, peaks characteristic of amorphous Si_3N_4 were observed in the Si2p$_{3/2}$ and Si2p$_{1/2}$ XPS region at 700 °C with a shift in binding energy to 102 eV.[36] The C1s peak became narrower with pyrolysis temperature, consistent with the conversion of Cp and methylene carbons to graphite at a binding energy of 285 eV. The results are consistent with the formation of more graphite with temperature as detected by PXRD.

High-resolution analysis of the Fe2p$_{3/2}$ XPS region of ceramics **5D** allowed the comparison of the amount of surface α-Fe to the amount of surface Fe_2O_3.[35] This surface Fe_2O_3 is present as a native oxide layer, which results from the presence of a small amount of adventitious oxygen in the polymer matrix. No Fe_2O_3 diffraction peaks were observed by PXRD, indicating that no bulk Fe_2O_3 was present. This supports the absence of significant amounts of oxygen during the pyrolysis. The surface α-Fe to surface Fe_2O_3 ratio decreases linearly with particle size. This suggests the α-Fe particles do not segregate on the surface but rather form in the bulk, inside the ceramic matrix; this provides further evidence that α-Fe catalyzed graphite formation is probable. High-resolution Fe2p$_{3/2}$ scans for the polymer **4** indicated that iron was present as ferrocenyl moieties (E_B = 708 eV) and as small amounts of Fe_2O_3 (E_B = 711 eV). As the temperature was increased, the ferrocenyl moieties degraded, and α-Fe (E_B = 707 eV) was formed initially at 600 °C, in **5D**$_{600\ °C-2\ h}$, and more significantly at 700 °C, in **5D**$_{700\ °C-2\ h}$. As the pyrolysis temperature was increased up to 1000 °C, the relative amount of external surface Fe as compared to the oxide layer is further decreased.

High-resolution spectra of the Si2p$_{3/2}$ and Si2p$_{1/2}$ XPS regions were also analyzed.[35] Initially, the Si2p peak was detected at E_B = 101 eV (polymer **4**), but with increased temperature a shift to higher binding energies (E_B = 103 eV) was observed, and at 700 °C (**5D**$_{700\ °C-2\ h}$) the formation of amorphous Si_3N_4 was detected. As the temperature was further increased to 850 °C, the formation of a small amount of SiC was observed at E_B = 99 eV (**5D**$_{850\ °C-2\ h}$). The SiC disappeared at 950 °C with the formation of more crystalline Si_3N_4 and graphite. This was consistent with the observed crystallization of silicon nitride at 950 °C by PXRD. We believe that the low reaction temperature between SiC and nitrogen is due to the catalytic effect of the iron particles present in the ceramics.

2.a.v. Magnetization Studies. As the ceramics prepared at ≥600 °C were attracted to a bar magnet, we were interested in correlating the magnetic properties of the materials with the α-Fe particle size. Samples prepared at 650 °C (**5D**$_{650\ °C-2\ h}$), 850 °C (**5D**$_{850\ °C-2\ h}$), and 1000 °C (**5D**$_{1000\ °C-2\ h}$) were analyzed by SQUID magnetometry (Figure 6). Magnetization versus field data obtained at 100 and 300 K for ceramics **5D**$_{650\ °C-2\ h}$ and

(36) Moulder, J. F.; Stickle, W. F.; Sobol, P. E.; Bomben, K. D. In *Handbook of X-ray Photoelectron Spectroscopy: A Reference Book of Standard Spectra for Identification and Interpretation of XPS Data*; Chastain, J., Ed.; Perkin-Elmer Corporation: Eden Prairie, MN, 1992.

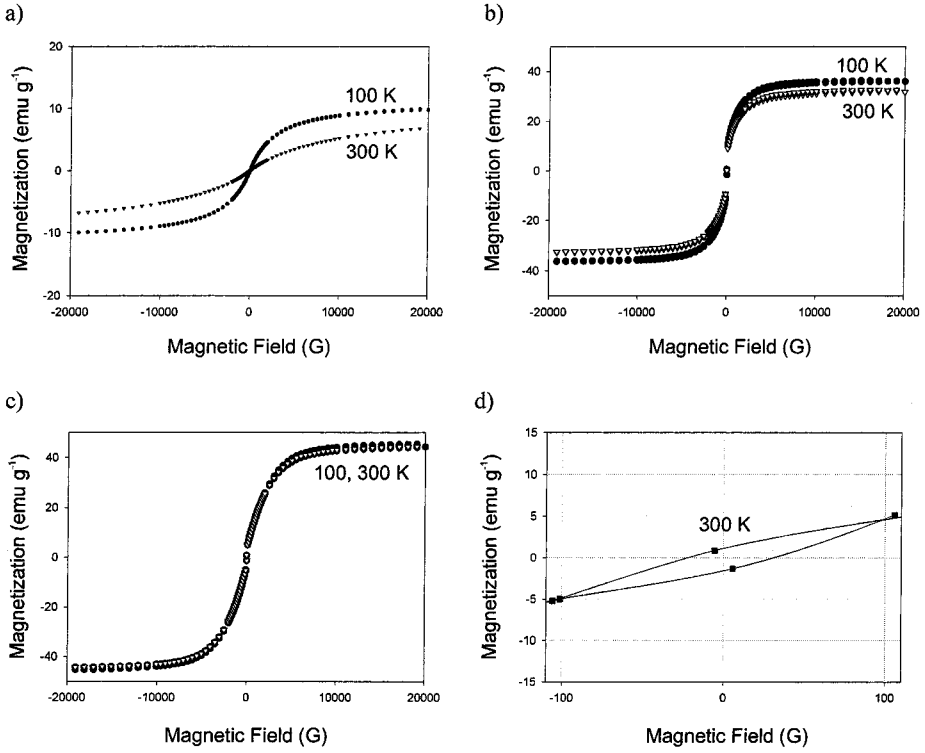

Figure 6. Magnetization versus magnetic field measurements conducted at 100 K (●) and 300 K (▽) for samples prepared at (a) 650 °C ($\mathbf{5D_{650\ °C-2\ h}}$), (b) 850 °C ($\mathbf{5D_{850\ °C-2\ h}}$), and (c) 1000 °C ($\mathbf{5D_{1000\ °C-2\ h}}$). (d) A magnified view of the magnetization curve in (c) obtained at 300 K. The ceramics $\mathbf{5D_{650\ °C-2\ h}}$ (a) and $\mathbf{5D_{850\ °C-2\ h}}$ (b) are superparamagnetic, and $\mathbf{5D_{1000\ °C-2\ h}}$ is ferromagnetic and displays room-temperature hysteresis (c and d).

$\mathbf{5D_{850\ °C-2\ h}}$ are shown in Figure 6a and b, respectively. Ceramics $\mathbf{5D_{650\ °C-2\ h}}$ and $\mathbf{5D_{850\ °C-2\ h}}$ contained small α-Fe particles (PXRD: 31 ± 6 Å in $\mathbf{5D_{650\ °C-2\ h}}$ and 92 ± 11 Å and 286 ± 9 Å in $\mathbf{5D_{850\ °C-2\ h}}$). The saturation magnetization for $\mathbf{5D_{650\ °C-2\ h}}$ was 7 emu g^{-1} at 300 K and 10 emu g^{-1} at 100 K; higher values were observed for $\mathbf{5D_{850\ °C-2\ h}}$ (32 emu g^{-1} at 300 K and 36 emu g^{-1} at 100 K) as expected with the presence of more iron particles. These samples showed no hysteresis at 100 or 300 K, and magnetic saturation was gradual, consistent with the behavior of superparamagnetic particles.

The magnetic behavior of the smaller α-Fe particles that were prepared below 900 °C can be compared with that of larger α-Fe particles prepared at 1000 °C (PXRD: 205 ± 51 Å and 606 ± 34 Å for $\mathbf{5D_{1000\ °C-2\ h}}$). For example, the magnetization of the larger α-Fe particles in ceramic $\mathbf{5D_{1000\ °C-2\ h}}$ rapidly reached saturation. The magnetization curves for $\mathbf{5D_{1000\ °C-2\ h}}$ at 100 and 300 K are shown in Figure 6c, with an enlarged view of the magnetization curve obtained at 300 K in Figure 6d; the ceramic possesses a saturation magnetization of 44 emu g^{-1} and coercive field of 10 G. Ceramic $\mathbf{5D_{1000\ °C-2\ h}}$ displayed room-temperature hysteresis and a small remnant magnetization (1 emu g^{-1}) consistent with a soft ferromagnet. This indicates that the α-Fe particles in $\mathbf{5D_{1000\ °C-2\ h}}$ had become large enough (larger than a single Weiss domain) to display ferromagnetism.[37] SQUID magnetometry thus demonstrated a transition from small superparamagnetic α-Fe particles to larger ferromagnetic α-Fe particles at ca. 900 °C. Therefore, by varying the pyrolysis temperature, the α-Fe particle size and magnetic properties of the resulting ceramics could be tuned. This flexibility may be advantageous for particular materials applications.

2.a.vi. Mössbauer Spectroscopic Studies. Mössbauer spectroscopic analysis was performed on several representative ceramic samples prepared at 650 °C ($\mathbf{5D_{650\ °C-2\ h}}$), 850 °C ($\mathbf{5D_{850\ °C-2\ h}}$), and 1000 °C ($\mathbf{5D_{1000\ °C-2\ h}}$) at 298, 90, and 4.2 K. SQUID measurements as described above identified the presence of superparamagnetic α-Fe particles in ceramic samples $\mathbf{5D_{650\ °C-2\ h}}$ and $\mathbf{5D_{850\ °C-2\ h}}$ prepared below 900 °C and larger ferromagnetic particles in ceramic $\mathbf{5D_{1000\ °C-2\ h}}$.

The results of Mössbauer spectroscopic analysis of the ceramics were broadly consistent with those of the magnetization studies. A Mössbauer spectroscopic study at 298 K of ceramic sample $\mathbf{5D_{650\ °C-2\ h}}$ showed two quadrupole doublets, each displaying intensity asymmetry (Figure 7a). The inner doublet possessed an isomer shift (IS) of 0.278 ± 0.006 mm s^{-1} and a quadrupole splitting (QS) of 0.849 ± 0.006 mm s^{-1}. The outer doublet possessed an IS of 0.402 ± 0.002 mm s^{-1} and QS 2.14 ± 0.01 mm s^{-1}. The spectrum obtained at 90 K is similar, but with the appearance of additional small peaks at ca. 2.6 and 0.5 mm s^{-1}. The spectrum obtained at 4.2 K (Figure 7b) shows an intense doublet consistent with the outer doublet observed at 298 and 90 K, as well as the coalescence of the inner doublet. The inner doublet is consistent with the presence of superparamagnetic Fe particles. This doublet results when fluctuating magnetic dipoles average the internal magnetic hyperfine field of the Fe nanoparticles. Below 90 K the ceramic passes through the blocking temperature and the quadrupole doublet undergoes coalescence, and broad peaks corresponding to magnetically ordered sites begin to appear at 4.2 K, as seen in Figure 7b. The broadness of the latter lines suggests that a situation involving complete magnetic hyperfine splitting has not been reached and that the particle size distribution has led to a

(37) The estimated maximum size of a single domain for a perfectly spherical Fe particle is 140 Å. Leslie-Pelecky, D. L.; Rieke, R. D. *Chem. Mater.* **1996**, *8*, 1770.

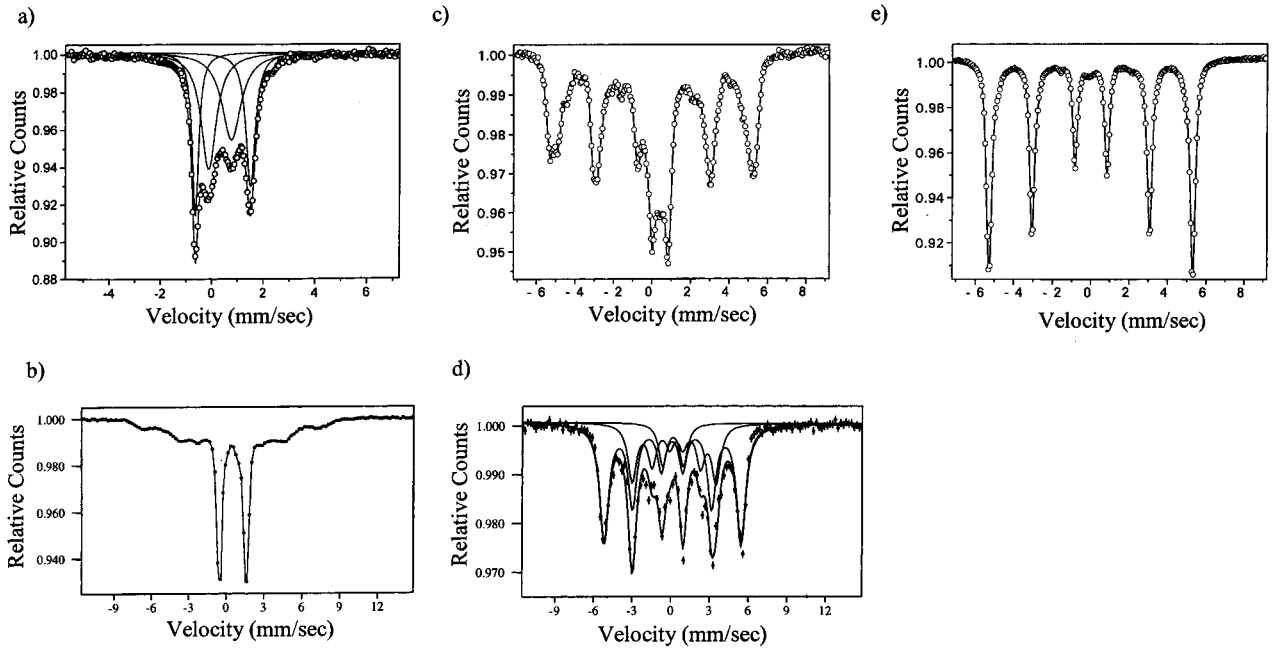

Figure 7. Mössbauer spectra of ceramics: $\mathbf{5D_{650\ °C-2\ h}}$ measured at (a) 298 K and (b) 4.2 K, $\mathbf{5D_{850\ °C-2\ h}}$ obtained at (c) 298 K and (d) 4.2 K, and (e) $\mathbf{5D_{1000\ °C-2\ h}}$ obtained at 298 K.

distribution of hyperfine fields. The outer doublet has Mössbauer spectral parameters similar to those for ferrocene (IS = 0.46 ± 0.01 mm s^{-1}, QS = 2.40 ± 0.01 mm s^{-1}).[38] The fact that the outer doublet is still present at 4.2 K indicates that it is most likely due to either a "ferrocene-like" environment present from residual polymer or even extremely small paramagnetic iron nanoclusters or matrix trapped iron atoms. However, the "ferrocene-like" assignment is not supported by the absence of d−d absorption and the C−H stretching overtone in reflectance UV−vis/near-IR spectroscopy, which indicate the absence of a ferrocenoid moiety in the ceramic lattice. A possible explanation takes account of the fact that both the d−d absorption and the C−H stretching first overtone are not allowed transitions and may be too weak and difficult to observe once most of the material has been converted to a ceramic containing α-Fe particles.

The Mössbauer spectra obtained at 298 K for the ceramic prepared at 850 °C ($\mathbf{5D_{850\ °C-2\ h}}$) revealed a doublet and two magnetically ordered subspectra (Figure 7c). The doublet was similar to the inner doublet of the 650 °C sample assigned to superparamagnetic Fe. The absence of the outer doublet seen in $\mathbf{5D_{850\ °C-2\ h}}$ showed that there is no iron present in a "ferrocene-like" environment, and this indicates that complete ceramic conversion was obtained at 850 °C. The magnetically ordered subspectra could be attributed to ferromagnetic α-Fe and another minor species with a smaller hyperfine field that may have a distribution of sites. The 90 K spectrum for $\mathbf{5D_{850\ °C-2\ h}}$ appears similar to the 298 K spectrum but with improved peak resolution. At 4.2 K the spectrum for $\mathbf{5D_{850\ °C-2\ h}}$ is quite complex and can be resolved into a small doublet and two magnetically ordered subspectra (Figure 7d). The doublet is consistent with that observed at 298 and 90 K and is assigned to very small superparamagnetic α-Fe particles above the blocking temperature. The magnetically ordered sites are attributed to the large α-Fe particles and to the superparamagnetic particles below their blocking temperature. The complexity of the spectra at 4.2 K may be attributed to a particle size distribution.

The Mössbauer spectra obtained for $\mathbf{5D_{1000\ °C-2\ h}}$ are virtually identical at 298 K (Figure 7e) and 90 K with a major magnetically ordered site due to ferromagnetic α-Fe and another subspectrum due to the presence of another minor magnetically ordered species. The absence of the smaller superparamagnetic

Table 3. Vickers Hardness and Young's Modulus for Polymer Network **4** and Ceramics **5D** Obtained from Nanoindentation Measurements

sample	pyrolysis temp (°C)	Vickers hardness (kg/mm²)	Young's modulus (GPa)
4		33.6 ± 0.3	6.9 ± 0.3
$\mathbf{5D_{500\ °C-2\ h}}$	500	45.2 ± 0.6	3.75 ± 0.06
$\mathbf{5D_{650\ °C-2\ h}}$	650	76 ± 3	6.9 ± 0.3
$\mathbf{5D_{750\ °C-2\ h}}$	750	17.5 ± 0.4	4.85 ± 0.04
$\mathbf{5D_{850\ °C-2\ h}}$	850	237 ± 2	29 ± 2
$\mathbf{5D_{1000\ °C-2\ h}}$	1000	97 ± 5	15.4 ± 0.4

Table 4. Scherrer Analysis of the (110) α-Fe Reflection and the Corresponding α-Fe Particle Sizes for Ceramics Prepared at Various Pyrolysis Times

ceramic sample	pyrolysis temp (°C)	pyrolysis time (h)	α-Fe particle size calculated from the (110) α-Fe reflection using the Scherrer equation (Å)[a]	
			small particle	large particles
$\mathbf{5D_{600\ °C-2\ h}}$	600	2		
$\mathbf{5D_{600\ °C-24\ h}}$	600	24	18.2 ± 0.4	
$\mathbf{5D_{700\ °C-0\ h}}$	700	0	15.0 ± 0.3	
$\mathbf{5D_{700\ °C-2\ h}}$	700	2	24.3 ± 0.7	257 ± 8
$\mathbf{5D_{700\ °C-8\ h}}$	700	8	37.4 ± 0.2	276 ± 9
$\mathbf{5D_{700\ °C-12\ h}}$	700	12	67.0 ± 6	272 ± 9
$\mathbf{5D_{700\ °C-24\ h}}$	700	24	62 ± 5	265 ± 8
$\mathbf{5D_{1000\ °C-2\ h}}$	1000	2	123 ± 19	637 ± 37
$\mathbf{5D_{1000\ °C-8\ h}}$	1000	8	129 ± 18	628 ± 36
$\mathbf{5D_{1000\ °C-24\ h}}$	1000	24	155 ± 29	680 ± 41

[a] The errors obtained for the values of fwhm (from the peak fitting software, Peakfit) were used to estimate the errors for the particle size values.

(38) Herber, R. H.; Temple, K.; Manners, I.; Buretea, M.; Tilley, T. D. *Inorg. Chim. Acta* **1999**, *287*, 152.

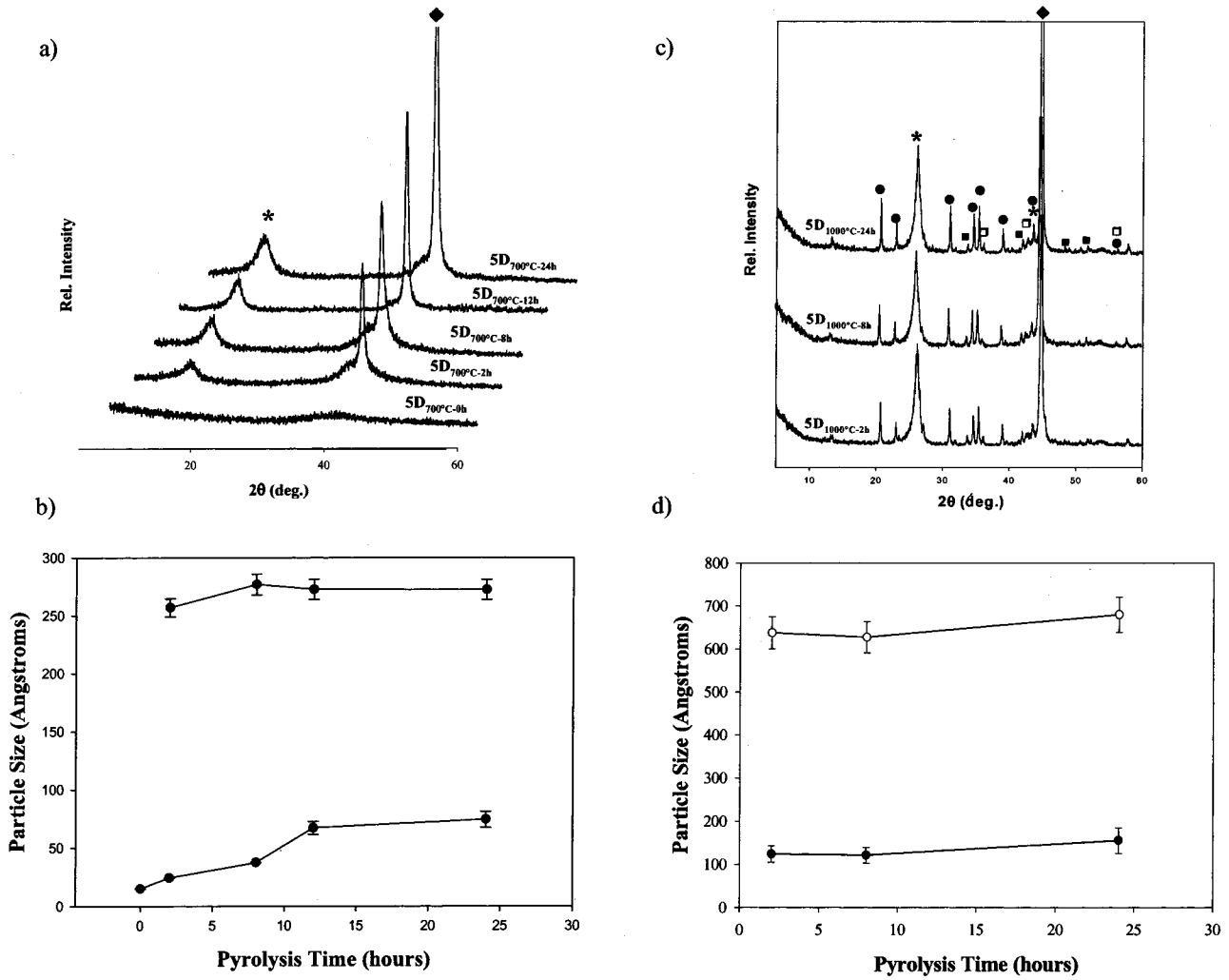

Figure 8. (a) PXRD patterns of ceramic samples $\mathbf{5D_{700\,°C-(0\,h-24\,h)}}$ prepared at 700 °C with pyrolysis times of 0, 2, 8, 12, and 24 h, respectively. (b) Plot of α-Fe particle size versus pyrolysis time. A bimodal particle size distribution occurred after pyrolysis for 2 h. (c) PXRD patterns of ceramic samples $\mathbf{5D_{700\,°C-(2\,h-24\,h)}}$ prepared at 1000 °C with pyrolysis times of 2, 8, and 24 h, respectively. (d) Plot of particle size versus pyrolysis time. The crystalline species present are α-Fe (◆), graphite (*), α-Si_3N_4 (●), Fe_4N (■), and Fe_2N (□).

particles is consistent with the observation of α-Fe particle growth with temperature.

2.a.vii. Nanoindentation Measurements. The mechanical properties of the ceramics were probed by nanoindentation studies on representative ceramic samples and the precursor polymer **4** for comparison. The results are tabulated in Table 3.

Ceramic $\mathbf{5D_{500\,°C-2\,h}}$, prepared at 500 °C, showed increased hardness (45.2 ± 0.6 kg/mm^2) as compared to polyferrocenylsilane precursor **4** (33.6 ± 0.3 kg/mm^2). With the formation of small α-Fe particles in $\mathbf{5D_{650\,°C-2\,h}}$, the hardness continued to increase (76 ± 3 kg/mm^2). The decreased hardness of ceramic $\mathbf{5D_{750\,°C-2\,h}}$ (17.5 ± 0.4 kg/mm^2) was likely due to the disruption of the polymer network, which is consistent with the observation of amorphous silicon nitride and crystalline graphite at 700 °C (XPS results). Further heating to 850 °C ($\mathbf{5D_{850\,°C-2\,h}}$) resulted in improved mechanical properties (237 ± 2 kg/mm^2) with the crystallization of α-Fe particles and Fe_4N. The combination of large α-Fe particles surrounded by more crystalline graphite for the sample prepared at 1000 °C ($\mathbf{5D_{1000\,°C-2\,h}}$) resulted in lower mechanical properties (97 ± 5 kg/mm^2) than in $\mathbf{5D_{850\,°C-2\,h}}$. The trends in modulus followed the same pattern as those for hardness. The only exception was that the Young's modulus decreased during the transition from polymer (6.9 ± 0.3 GPa) to ceramic $\mathbf{5D_{500\,°C-2\,h}}$ (3.75 ± 0.06 GPa). This was likely due to the initial expansion and transformation of the polymer network.

Of the ceramic samples, the one prepared at 850 °C possessed the most impressive mechanical properties with significant modulus and hardness (29 ± 2 GPa, 237 ± 2 kg/mm^2) greater than that of graphite (4.8 GPa, 12 kg/mm^2), copper (16.0 GPa, 163 kg/mm^2), and Borax glass (17.5 GPa, 199 kg/mm^2).[39]

2.b. Variation of Pyrolysis Time. A more limited series of experiments was conducted in which pyrolysis times were varied at selected temperatures. The goal was to investigate the rate of α-Fe nucleation and growth in the transforming matrix. Three temperatures were selected on the basis of the results of the variable pyrolysis temperature studies: 600 °C, where small α-Fe particles were first observed; 700 °C, where crystalline α-Fe and graphite were detected; and 1000 °C, where five different crystalline species were present. Details of the pyrolysis

(39) (a) Lide, D. R., Frederikse, H. P. R., Eds. *CRC Handbook of Chemistry and Physics*, 76th ed.; CRC Press: Boca Raton, FL, 1995. (b) Shackelford, J. F., Alexander, W., Park, J. S., Eds. *CRC Materials Science and Engineering Handbook*, 2nd ed.; CRC Press: Boca Raton, FL, 1994.

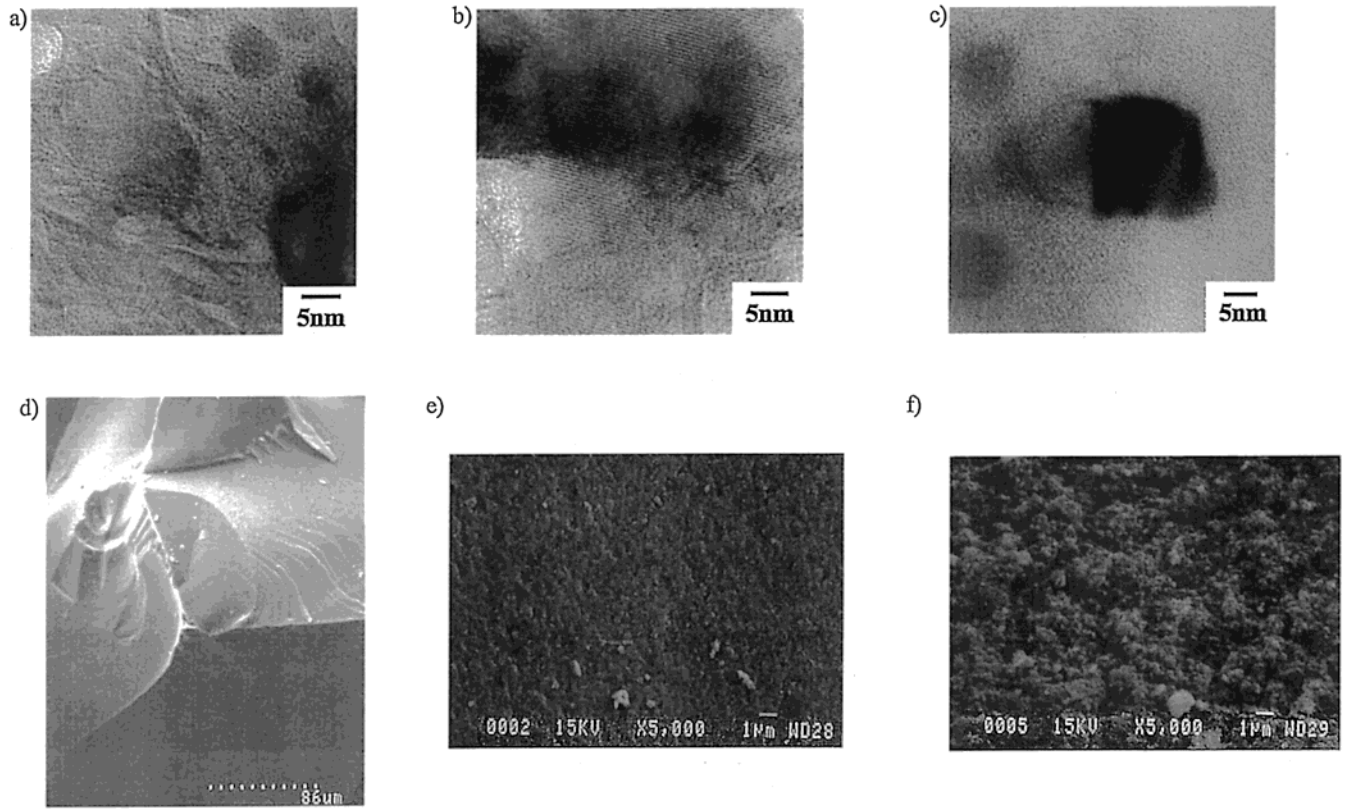

Figure 9. High-resolution lattice TEM images of ceramics treated for 24 h at (a) 700 °C (**5D**$_{700\ °C-24\ h}$), and (b) 1000 °C (**5D**$_{1000\ °C-24\ h}$) and (c) for **5F**$_{550\ °C-1\ h}$. SEM images of ceramics treated for 2 h at 600 °C (**5D**$_{600\ °C-2\ h}$) (d), and 24 h at (e) 700 °C (**5D**$_{700\ °C-24\ h}$), and (f) 1000 °C (**5D**$_{1000\ °C-24\ h}$).

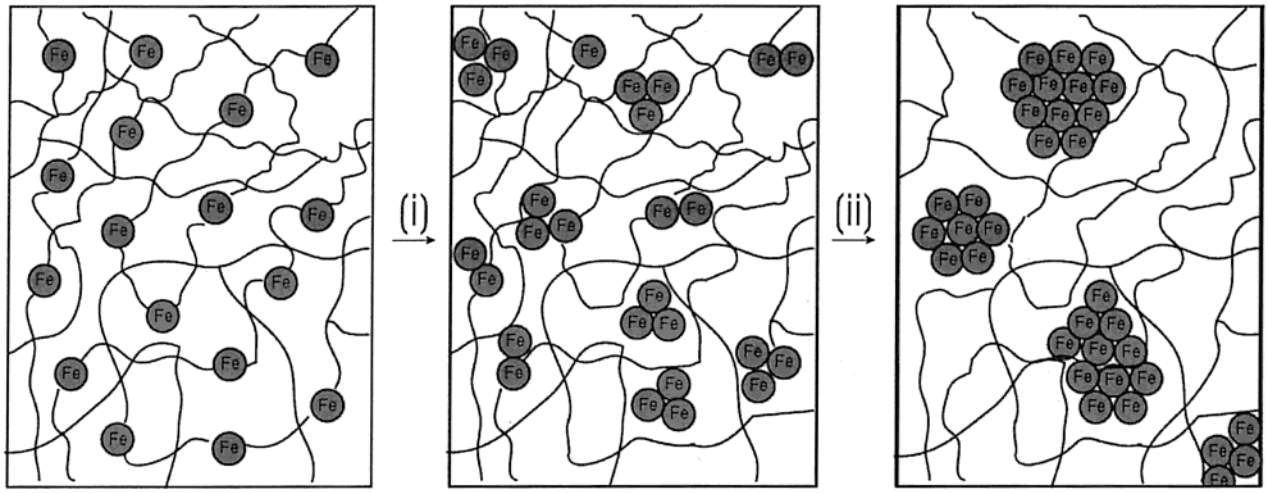

Figure 10. Graphical representation of a nucleation and growth model that illustrates the genesis of the magnetic ceramic **5** from (i) iron atom release from polymer **4** followed by (ii) nucleation and growth of iron nanoparticles.

conditions and ceramic yields are given in Table 1. In each case, samples were heated to the appropriate temperature over 1 h and then held constant for the respective time. The ceramics were investigated by PXRD, TEM, and SEM.

2.b.i. PXRD Studies. As in the previous section 2.a.i., the α-Fe particle sizes were calculated from the measured peak widths for the (110) reflection of α-Fe using the Scherrer equation, and the values are summarized in Table 4. The PXRD patterns for ceramics prepared at 600 °C showed only a very broad peak at $2\theta = 45°$ after 2 h, and a sharper peak after 24 h, characteristic of nanocrystalline α-Fe particles.[35] Because of the low intensity of the α-Fe peak for **5D**$_{600\ °C-2\ h}$, it was not possible to calculate an average particle size. However, **5D**$_{600\ °C-24\ h}$ showed a sharper peak consistent with that of α-Fe particles of size 18.2 ± 0.4 Å (monomodal). Graphite did not crystallize at this temperature, even after 24 h.

Figure 8a shows PXRD patterns of ceramic samples **5D** that were prepared at 700 °C. The temperature was held at 700 °C for 0 h (**5D**$_{700\ °C-0\ h}$), 2 h (**5D**$_{700\ °C-2\ h}$), 8 h (**5D**$_{700\ °C-8\ h}$), 12 h (**5D**$_{700\ °C-12\ h}$), and 24 h (**5D**$_{700\ °C-24\ h}$). The α-Fe particle size and sample crystallinity increased with pyrolysis time (Table 4). Ceramic **5D**$_{700\ °C-0\ h}$, which was heated to 700 °C and then

permitted to cool, showed a broad peak corresponding to 15.0 ± 0.3 Å α-Fe particles. After 2 h (**5D**$_{700\ °C-2\ h}$) of pyrolysis, a bimodal α-Fe particle size distribution resulted. With extended heating to 24 h (**5D**$_{700\ °C-24\ h}$), the crystallinity of both α-Fe and graphite increased, suggesting that α-Fe particles catalyzed the formation of graphite at 700 °C. Figure 8b shows a plot of the α-Fe particle size as a function of time. There was a linear growth in particle size for the small α-Fe particles, and the large particles grew until they reached a critical size after ca. 8 h. As well, it should be noted that the intensity of the α-Fe reflection increases with temperature as more iron particles are formed. Iron and silicon nitrides were observed after 850 °C in the studies as a function of pyrolysis temperature (section 2.a.). However, nitrides were not observed in **5D**$_{700\ °C-24\ h}$ formed at 700 °C despite a pyrolysis time of 24 h.

Figure 8c shows the PXRD patterns of ceramic samples prepared at 1000 °C for 2 h (**5D**$_{1000\ °C-2\ h}$), 8 h (**5D**$_{1000\ °C-8\ h}$), and 24 h (**5D**$_{1000\ °C-24\ h}$). All of the ceramics contained the same crystalline components: α-Fe, graphite, α-Si_3N_4, Fe_4N, and Fe_2N, with intensities increasing with pyrolysis time. Figure 8d shows a bimodal particle size distribution of α-Fe particles, with the average particle sizes for both the small and the large particles remaining constant with temperature; however, there is an increase in the intensity of the α-Fe reflection indicating an increase in the number of particles. Therefore, at 1000 °C α-Fe particles rapidly reached their size limit, and the size then remained constant (Figure 8d) though the number of particles increased.

2.b.ii. TEM and SEM Analysis. High-resolution TEM images were obtained for **5D**$_{700\ °C-24\ h}$, **5D**$_{1000\ °C-24\ h}$, and **5F**$_{550\ °C-1\ h}$ (Figure 9a−c). From the lattice images graphite was identified in **5D**$_{700\ °C-24\ h}$ (Figure 9a) and **5D**$_{1000\ °C-24\ h}$ (Figure 9b) with a lattice spacing of 3.4 Å. Graphite was present in abundance in **5D**$_{1000\ °C-24\ h}$ and appeared to "encapsulate" the α-Fe particles. Similarly, the α-Fe particles in ceramic film **5F**$_{550\ °C-1\ h}$ (Figure 9c) also appeared to be embedded in a graphite shell. This shell of graphite may protect the Fe nanoparticles from oxidation upon exposure to air. This observation was consistent with the proposed catalysis of graphite formation by the α-Fe nanoparticles.

Figure 9d−f shows SEM micrographs of **5D**$_{600\ °C-2\ h}$, **5D**$_{700\ °C-24\ h}$, and **5D**$_{1000\ °C-24\ h}$ pyrolyzed for 2 h at 600 °C and 24 h at 700 and 1000 °C, respectively. Figure 9d shows a smooth and nonporous ceramic surface, the lack of porosity being confirmed by nitrogen adsorption measurements at 77 K. A SEM of **5D**$_{700\ °C-24\ h}$ (Figure 9e) shows a smooth surface, whereas the formation of external surface α-Fe crystallites was apparent in **5D**$_{1000\ °C-24\ h}$ (Figure 9f), accounting for the rough nature of the surface in this ceramic.

3. A Model for Ceramic Formation. A model showing how the genesis of magnetic ceramic from cross-linked polyferrocenylsilane depends on pyrolysis conditions is presented in Figure 10. Upon heating the cross-linked polymer **4**, expansion of the network occurred, as observed by variable temperature PXRD at 250 °C. Further heating resulted in Fe atom "release" from the ferrocene moieties. UV−vis/near-IR spectroscopy showed the disappearance of ferrocene units by 650 °C, though this result is tentative as the results might have been influenced by the absorption of the semimetallic ceramic. The polymer matrix was dismantled as nucleation and growth of the α-Fe

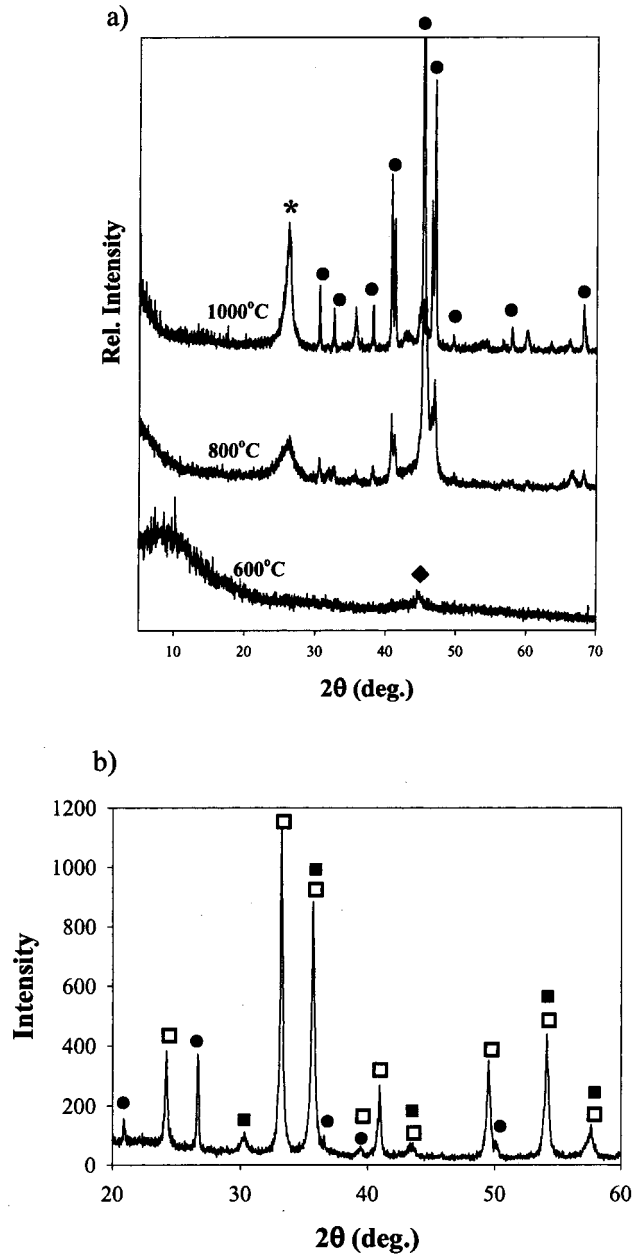

Figure 11. (a) PXRD patterns of ceramics **6**$_{600\ °C-2\ h}$, **6**$_{800\ °C-2\ h}$, and **6**$_{1000\ °C-2\ h}$ prepared under an argon atmosphere. The crystalline species observed were α-Fe nanoparticles (◆), graphite (*), and Fe_5Si_3 (●). (b) PXRD pattern of **7**, prepared by pyrolysis under air. The species present were hematite (Fe_2O_3, □), quartz (SiO_2, ●), and maghemite C (Fe_2O_3, ■).

particles occurred. Mössbauer spectroscopy showed the "ferrocene-like" species disappear above 650 °C. Disappearance of polymer order before 600 °C as detected by PXRD coincided with the initial observation of α-Fe particles. At 700 °C, the α-Fe particles appeared to catalyze the formation of graphitic ribbons in the ceramic; both species then continued to grow in size with temperature. The α-Fe particles form with a bimodal particle size distribution possibly due to the formation of larger particles at grain boundaries and defect sites as a result of faster intergrain iron atom diffusion. N1s XPS studies of the ceramic showed the incorporation of nitrogen at 700 °C, which was later incorporated into crystalline silicon and iron nitrides as observed by PXRD. A small amount of Fe_4N formed at 850 °C and appeared to be localized at the ceramic surface. This "competi-

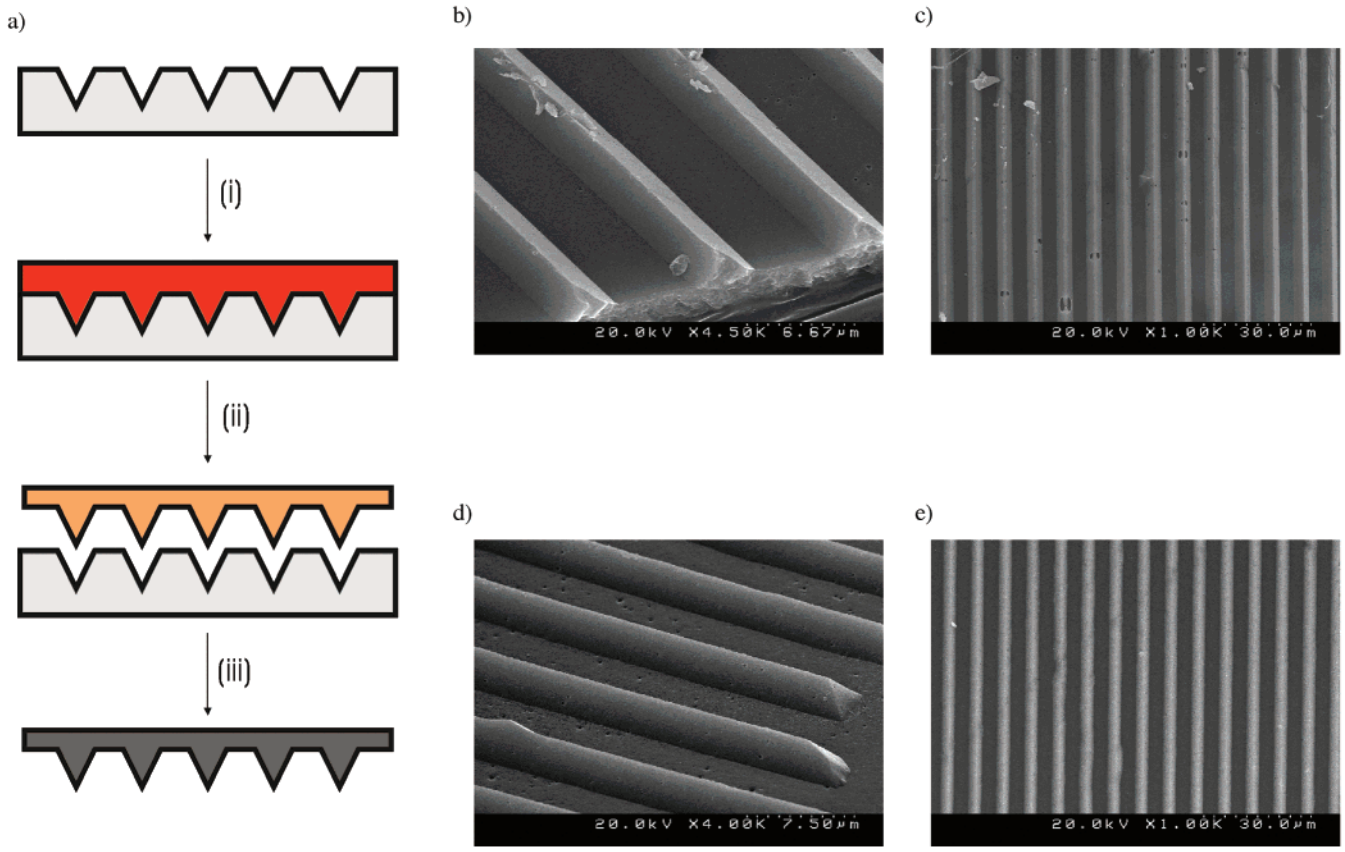

Figure 12. (a) Schematic representation of the micron scale patterning of **4** and the formation of ceramic **5**. (i) A concentrated solution of monomer **3** in CH_2Cl_2 was dropped onto the silicon substrate with a silicon oxide surface layer, and the solvent was allowed to evaporate leaving behind a monomer film. (ii) Heating at 200 °C for 12 h under N_2 yielded polymer **4**, which was separated from the silicon substrate by etching the middle silicon oxide layer with 1 wt % HF. (iii) A piece of the free-standing patterned polymer film was pyrolyzed at 600 °C under nitrogen to form the patterned ceramic film **5**. (b) and (c) show SEM images of the patterned polymer film **4**, and (d) and (e) show the resulting ceramic film **5**.

tion" for Fe atoms appears to cause a decrease in α-Fe particle size at 900 °C, which was followed by the crystallization of α-Si_3N_4 and a small amount of Fe_2N at 950 °C. Magnetic measurements demonstrated that as the α-Fe particles became larger, they underwent the expected transition from superparamagnetic to ferromagnetic behavior. Particles formed below 900 °C contained α-Fe particles that were smaller than a single Weiss domain and behaved as superparamagnets, whereas larger particles prepared at 1000 °C conferred ferromagnetic properties to the ceramic.

4. Influence of Different Pyrolysis Atmospheres: Pyrolysis of Polyferrocenylsilane Network 4 Under Argon and Air. The last pyrolysis condition to be varied was the atmosphere. The incorporation of nitrogen from the pyrolysis atmosphere clearly showed that the ceramic composition depends on the surrounding gas during pyrolysis. Ceramics **6** and **7** were prepared under argon and air, respectively, and were studied by PXRD.

Bulk samples $\mathbf{6}_{600\,^\circ C-2\,h}$, $\mathbf{6}_{800\,^\circ C-2\,h}$, and $\mathbf{6}_{1000\,^\circ C-2\,h}$ were prepared under an argon atmosphere for 2 h at 600 , 800, and 1000 °C, respectively. Ceramics **6** were obtained in 81−89% ceramic yield and showed shape retention. These ceramics were also attracted to a bar magnet. Figure 11a shows the PXRD patterns of ceramic samples **6**; initially $\mathbf{6}_{600\,^\circ C-2\,h}$ shows the (110) α-Fe reflection, corresponding to an average nanoparticle size of 48 ± 2 Å. With further heating, the α-Fe nanoparticles react with their surrounding matrix to form crystalline Fe_5Si_3 and crystalline graphite ($\mathbf{6}_{800\,^\circ C-2\,h}$). With higher temperatures ($\mathbf{6}_{1000\,^\circ C-2\,h}$), the intensity of these crystalline components increased. Previous reports by Corriu and co-workers showed the formation of Fe_3Si from pyrolysis of 2,5-disilahexane/iron carbonyl organometallic precursors.[22c] To our knowledge, the preparation of ceramics **6** represents the first polymer precursor route to Fe_5Si_3.

Polymer **4** was also pyrolyzed under a gentle flow of air for 2 h at 1000 °C. The pyrolysis resulted in a red ceramic $\mathbf{7}_{1000\,^\circ C-2\,h}$ in moderate (53%) yield. The crystalline components were identified as quartz (SiO_2), hematite (Fe_2O_3), and maghemite C (Fe_2O_3), as shown in Figure 11b.

5. Micron Scale Patterning of the Cross-Linked Polyferrocenylsilane 4 and the Magnetic Ceramic 5 using Micromolding Techniques Inside Silicon Wafers. With the knowledge that shaped macroscopic ceramics can be formed from **4** and our now detailed understanding of the nature of the nanostructured magnetic materials, we expanded the application of the polyferrocenylsilane precursor approach to micron scale patterning. Si(100) wafers patterned by microcontact printing SAMs of alkanethiols on gold followed by selective wet etching[29] were used to form patterned microscale designs of the cross-linked polyferrocenylsilane network **4**, as well as the magnetic ceramic **5**, illustrated in Figure 12a. A monomer film formed through solution casting underwent thermal ROP to form a red polymer film. Using a dilute HF solution, the oxide layer between the polymer film and the Si wafer was dissolved,

permitting lift-off and isolation of a free-standing polymer film. The surface pattern was imaged by SEM (Figure 12b−c); it is evident that the polymer film replicated the triangular grooves patterned on the Si wafer. The separation between the apices is 8.3 μm, and the triangle base width is 4.1 μm. The pyrolysis of a portion of the polymer film yielded a ceramic film. SEM of the ceramic is shown in Figure 12d−e, illustrating the shape retention of the polymer without the presence of a mold during pyrolysis; the apex separation and base width are 7.6 and 3.6 μm respectively (ca. 10% shrinkage).

Summary and Conclusion

The pyrolysis of cross-linked polyferrocenylsilane **4** gave shaped macroscopic magnetic ceramics in which α-Fe nanoparticles were encapsulated in a $SiC/C/Si_3N_4$ matrix. The matrix hosted the controlled release of iron atoms and nucleation and growth of iron nanoparticles. Moreover, the pyrolysis, temperature, time, and atmosphere strongly affected the composition and properties of the resulting ceramics.

Varying pyrolysis temperature and time permitted the study of α-Fe particle growth. Magnetization data showed that the smaller α-Fe particles in ceramics prepared at 650 and 850 °C exhibited superparamagnetic behavior, whereas larger particles in materials prepared at 1000 °C displayed ferromagnetic behavior. Through interpretation of our data, we proposed a model for ceramic formation from the polyferrocenylsilane network. We have also shown that micromolding of the spirocyclic [1]ferrocenophane precursor within soft lithographically patterned and anisotropically etched channels housed inside silicon wafers can be utilized to create micron scale designs of the cross-linked polyferrocenylsilane network polymer precursor as well as the magnetic ceramic product.

In conclusion, we have reported the first investigation of the genesis of a magnetically tunable ceramic from a well-defined metal-containing polymer network, which allows shape retention of monolithic shaped objects and micron scale patterned materials to be formed. The approach reported may ultimately be useful in the formation of "ceramic materials with controlled form", which may prove to be of interest in magnetic recording, magnetically tunable photonics, magnetic refrigeration, and magnetic shielding applications.

Acknowledgment. We are grateful to Professor G. M. Whitesides and Dr. H. Yang (Department of Chemistry and Chemical Biology, Harvard University) for providing the lithographic photoresist master. We acknowledge Dr. S. Petrov (Department of Chemistry, University of Toronto) for his help with PXRD studies, Dr. C. Berry (Department of Materials Science and Engineering, McMaster University) for gas adsorption measurements, and Dr. G. Favoro (Applications Laboratory, CSEM Instruments, Neuchatel, Switzerland) for nanoindentation measurements and calculations. We thank the Natural Sciences and Engineering Research Council of Canada (NSERC) for a post-graduate scholarship (1995−99, M.J.M.) and an E. W. R. Steacie Fellowship (1997−99, I.M.), and the Canadian Government for a Canada Research Chair in Materials Chemistry (2001−2008, G.A.O.) and a Canada Research Chair in Inorganic and Polymer Chemistry (2001−2008, I.M.). I.M. thanks the Ontario Government for a PREA Award (1999−2004) and the University of Toronto for a McLean Fellowship (1997−2003).

Supporting Information Available: Reflectance UV−vis/near-IR and XPS data for polymer **4** and ceramics **5D** and PXRD patterns for ceramics $\mathbf{5D}_{600\ °C-(2\ h-24\ h)}$ (PDF). This material is available free of charge via the Internet at http://pubs.acs.org.

JA0107273